

Transglutaminase 2 has higher affinity for relaxed than for stretched fibronectin fibers

Journal Article**Author(s):**

Selcuk, Kateryna; Leitner, Alexander; Braun, Lukas; Blanc, Fanny Le; Pacak, Paulina; Pot, Simon; Vogel, Viola

Publication date:

2024-01

Permanent link:

<https://doi.org/10.3929/ethz-b-000650893>

Rights / license:

[Creative Commons Attribution 4.0 International](#)

Originally published in:

Matrix Biology 125, <https://doi.org/10.1016/j.matbio.2023.12.006>

Funding acknowledgement:

175839 - Mechanobiology of Extracellular Matrix (SNF)



Transglutaminase 2 has higher affinity for relaxed than for stretched fibronectin fibers

Kateryna Selcuk^a, Alexander Leitner^b, Lukas Braun^a, Fanny Le Blanc^{b,1}, Paulina Pacak^a, Simon Pot^{a,2}, Viola Vogel^{a,*}

^a Department of Health Sciences and Technology, Institute of Translational Medicine, Laboratory of Applied Mechanobiology, ETH Zurich, Gloriastrasse 37-39 GLC G11, CH-8092 Zurich, Switzerland

^b Department of Biology, Institute of Molecular Systems Biology, ETH Zurich, Otto-Stern-Weg 3, CH-8093 Zurich, Switzerland

ARTICLE INFO

Keywords:

Mechanobiology
Cell-ECM reciprocity
Conformational switch
Cancer
Fibrosis
Transglutaminase 2 (TG2)

ABSTRACT

Transglutaminase 2 (TG2) plays a vital role in stabilizing extracellular matrix (ECM) proteins through enzymatic crosslinking during tissue growth, repair, and inflammation. TG2 also binds non-covalently to fibronectin (FN), an essential component of the ECM, facilitating cell adhesion, migration, proliferation, and survival. However, the interaction between TG2 and fibrillar FN remains poorly understood, as most studies have focused on soluble or surface-adsorbed FN or FN fragments, which differ in their conformations from insoluble FN fibers. Using a well-established in vitro FN fiber stretch assay, we discovered that the binding of a crosslinking enzyme to ECM fibers is mechano-regulated. TG2 binding to FN is tuned by the mechanical tension of FN fibers, whereby TG2 predominantly co-localizes to low-tension FN fibers, while fiber stretching reduces their affinity for TG2. This mechano-regulated binding relies on the proximity between the N-terminal β -sandwich and C-terminal β -barrels of TG2. Crosslinking mass spectrometry (XL-MS) revealed a novel TG2-FN synergy site within TG2's C-terminal β -barrels that interacts with FN regions located outside of the canonical gelatin binding domain, specifically FN_{I2} and FNIII₁₄₋₁₅. Combining XL-MS distance restraints with molecular docking revealed the mechano-regulated binding mechanism between TG2 and modules FN_{I7-9} by which mechanical forces regulate TG2-FN interactions. This highlights a previously unrecognized role of TG2 as a tension sensor for FN fibers. This novel interaction mechanism has significant implications in physiology and mechanobiology, including how forces regulate cell adhesion, spreading, migration, phenotype modulation, depending on the tensional state of ECM fibers. Data are available via ProteomeXchange with identifier PXD043976.

Introduction

The growing field of mechanobiology has revealed that not only the biochemical, but also the physical properties of the extracellular matrix (ECM) have a major impact on cell decision making in development, hemostasis and wound healing [1–4], and when altered can drive pathological transformations, including cancer and fibrotic pathologies [5]. Enzymatic crosslinking of ECM fibers is necessary for the mechanical stabilization during tissue growth and repair, but also plays major roles as the driver of fibrotic diseases and malignancy [6–8]. Transglutaminase 2 (TG2), also referred to as tissue transglutaminase, is

mostly retained within the cell under homeostatic conditions, but upon tissue injury or inflammation, its expression and subsequent export to the cell surface and the extracellular environment are strongly upregulated [9–12]. Once secreted, TG2 alters the physico-chemical properties of the extracellular environment by enzymatically crosslinking various ECM proteins, making the ECM stiffer and more resistant to proteolytic degradation. In turn, this triggers various downstream effects which change cell behavior and promote cell adhesion, migration and fibroblast proliferation [11,13]. While these processes are essential to stabilize the provisional ECM during wound healing, they need to be tightly regulated, and aberrant TG2 activity leads to pathological fibrosis [6,14,

* Corresponding author at: Department of Health Sciences and Technology, Institute of Translational Medicine, Laboratory of Applied Mechanobiology, ETH Zurich, Gloriastrasse 37-39 GLC G12.2, CH-8092 Zurich, Switzerland.

E-mail address: viola.vogel@hest.ethz.ch (V. Vogel).

¹ Present address: Master de Biologie, École Normale Supérieure de Lyon, Université Claude Bernard Lyon 1, Université de Lyon, 69342 Lyon Cedex 07, France

² Present address: Ophthalmology Section, Equine Department, Vetsuisse Faculty, University of Zurich, Winterthurerstrasse 260, 8057 Zurich, Switzerland

<https://doi.org/10.1016/j.matbio.2023.12.006>

Received 31 July 2023; Received in revised form 20 November 2023; Accepted 18 December 2023

Available online 20 December 2023

0945-053X/© 2023 The Authors. Published by Elsevier B.V. This is an open access article under the CC BY license (<http://creativecommons.org/licenses/by/4.0/>).

15]. Indeed, it was shown in healthy tissues that most externalized TG2 is catalytically inactive and only transiently activated by stress signals [16,17]. However, the crosslinking activity is only one component of the large functional arsenal of TG2. Numerous studies have shown that it also acts as a non-enzymatic scaffold protein that interacts with many ECM components and cell-surface receptors, such as fibronectin, collagen, vitronectin, integrins, syndecan-4, several growth factor receptors and others, to support cell adhesion, migration, proliferation and survival [18,19].

Fibronectin (FN) is one of the best characterized binding partners of TG2 in the ECM, which is overexpressed during development, tissue growth and repair as well as under various pathological conditions. Dimeric FN polymerizes to form fibrous matrices that promote cell adhesion, migration, and proliferation. Usually, cells adhere to FN through transmembrane receptors called integrins through the Arg-Gly-Asp (RGD) integrin binding site on FNIII₁₀ and additionally the synergy site on FNIII₉, which is selectively recognized by integrin α 5 β 1. However, RGD-dependent cell adhesion and the associated outside-in integrin signaling may be disrupted during extensive tissue damage and ECM remodeling. Blocking of the cell adhesion with synthetic RGD-peptides causes reduction of FN-integrin interaction and in the absence of TG2 leads to detachment-induced apoptosis (anoikis) in many cell types [14,19,20]. However, when TG2 is expressed on the cell surface, it can rescue cells from anoikis when RGD-dependent adhesion is blocked, thereby promoting cell survival [14,20–22]. This rescue does not depend on the enzymatic activity of TG2, but requires FN-binding together with the assistance of Syndecan-4's heparan sulfate chains and/or non-canonical binding to β 1-integrins [14,20,23]. Furthermore, TG2-FN interaction enhances deposition of FN fibers with assistance of Syndecan-4 and β 1-integrins, when RGD-dependent adhesion is attenuated, thus helping to quickly restore the extracellular environment after injury [22,24]. Finally, TG2 also binds to the Stachel, which is the extracellular domain of adhesive GPCRs [25].

Given the pro-survival adhesive properties of the TG2-FN complex, it

is not surprising that high expression levels of TG2 favor metastasis formation in multiple cancers [8,26–31]. Consequently, TG2 upregulation in these tumors is strongly associated with poor patient outcome [32]. This makes the TG2-FN complex a compelling drug target [7,13]. Currently, efforts are underway to develop small molecule inhibitors that disrupt the TG2-FN interface [33–36]. Thus, a deeper mechanistic and structural understanding of the TG2-FN interaction sites would not only shed light on its role in wound healing and cancer, but it would also assist the rational design of drugs.

TG2 consists of four domains: an N-terminal β -sandwich, a catalytic core, and two C-terminal β -barrels (Fig. 1A). While previous structural studies have characterized TG2 in two conformational states ("open" and "closed") using crystallography [37,38], evidence suggests that these two states do not adequately capture the protein's conformational plasticity. When TG2 is bound to GDP, GTP or other purine nucleotides, it adopts an enzymatically inactive "closed" conformation. In this state, the C-terminal β -barrel domains tightly fold over the catalytic domain, obstructing access to the active site (PDB:1KV3) [38] (Fig. 1B). However, when the active site is covalently bound to an irreversible inhibitor Z-DON, TG2 undergoes a large conformational change (PDB:2Q3Z) [37]. The β -barrel domains are prevented from interacting with the catalytic core, resulting in an "open", extended conformation (Fig. 1B). Although the PDB:2Q3Z conformation is often associated with the catalytically active TG2 due to the readily accessible active site, there are doubts regarding its true representation of the active form [39]. Firstly, PDB:2Q3Z contains a Cys370-Cys371 disulfide bridge near the active site, which if formed inhibits TG2 catalytic activity [40,41]. Secondly, the formation of this disulfide bridge induces local changes in the peptide backbone conformation, disrupting the calcium binding sites [41]. Consequently, the PDB:2Q3Z structure, bound to Z-DON inhibitor, does not include any calcium ions, despite their known requirement for its crosslinking function [37]. Finally, no crystal structure of catalytically active TG2 bound to calcium ions has been solved to date. Therefore, it is unlikely that the extended conformation observed in the

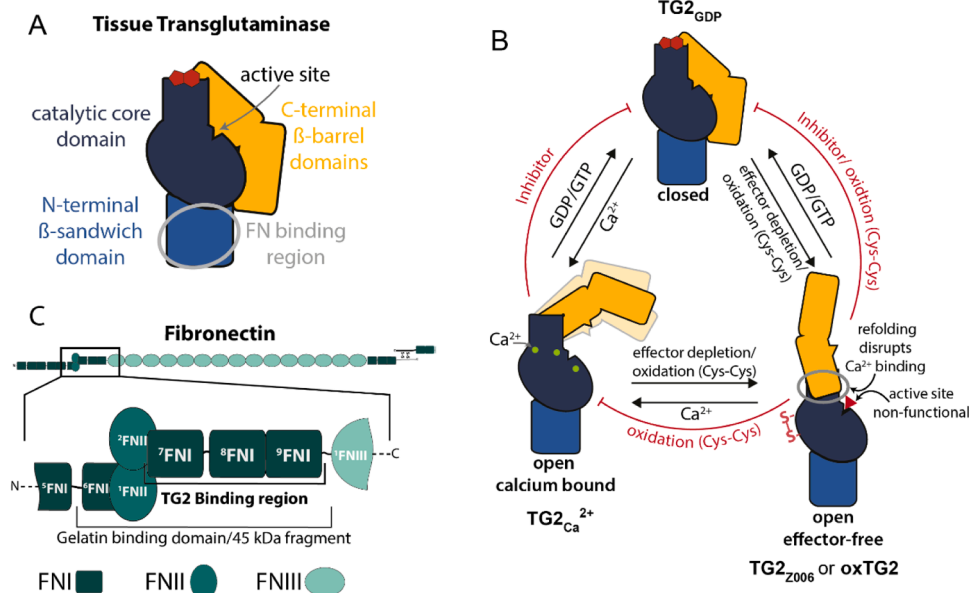


Fig. 1. Schematic illustration of TG2's domain composition, its conformational states and known binding interactions with fibronectin (FN). A: Schematic view of TG2's domain architecture based on the crystal structure of the catalytically inactive, GDP bound state (PDB:1KV3) [38]. The FN binding region on the N-terminal domain determined by Cardoso et al. is highlighted [44]. B: TG2 can exist in an equilibrium of at least three distinct conformational states: closed - TG2_{GDP}, open calcium bound - TG2_{Ca²⁺} and open effector-free state. The relative population of each state depends on the concentration of its allosteric effectors, with calcium (green circles), TG2_{Ca²⁺} and GDP/GTP (red polygons) and TG2_{GDP}, and can be further regulated by the formation of intramolecular disulfide bridges (oxidation - oxTG2) or the binding of artificial irreversible inhibitor Z-DON (red triangle) to the active site Cys277 (TG2_{Z006}). C: Illustration of the domain architecture of FN. Only one chain of the disulfide-linked FN homodimer is fully shown (top). The TG2 binding region in the gelatin binding domain determined by Soluri et al. (FN type I modules 7–9) is highlighted in the zoom-in [45].

Z-DON inhibitor-bound TG2 structure accurately represents the calcium-bound catalytically active protein. Indeed, small angle X-ray/neutron scattering (SAXS/SANS), hydrogen-deuterium exchange (HDX) and biosensor measurements suggest that the calcium bound TG2 assumes an “open” conformation distinct from the two known structures [41–43]. The reversible formation of the Cys370-Cys371 disulfide bond acts as a redox switch, inactivating TG2 in the oxidative environment of the ECM and desensitizing it to the presence of effectors [40]. In fact, experimental evidence indicates that the Z-DON inhibitor-bound structure resembles the oxidized TG2, i.e. TG2 in the extended effector-free state [41,43]. Thus, TG2 can adopt more than the two crystallographically captured conformations and exists in at least three different states: nucleotide binding favors the “closed” conformation [38], while high calcium concentrations predominantly induce the “open” but currently unknown conformation [41,43]. Importantly, only this open state with currently unknown conformation is catalytically active. In the absence of calcium or GDP/GTP and under oxidative conditions, TG2 assumes the structurally resolved, catalytically inactive “open” effector-free state [41] (Fig. 1B).

While significant progress has been made towards mapping of the interactions between TG2 and FN, previous studies that sought to investigate TG2-FN interactions were either performed with soluble dimeric FN or with shorter FN fragments [21,44–49]. Thus, nothing is known about how FN fibrillogenesis might affect its interactions with TG2. Soluble dimeric FN, as well as many of its fragments, adopts a quaternary structure, which is distinct from the insoluble fibrillar form in the ECM [50–52]. Although the exact structure of the fibrillar FN remains unknown, mutagenesis and then a super-resolution microscopy study has shown that that FN fibrillogenesis requires the N-terminal Fn_{1–5} domains [53] and that FN polymerizes in an antiparallel fashion with an N-terminal overlap of almost 40 nm [54]. Cell-mediated stretching of FN fibers during FN fibrillogenesis can either create additional interaction sites for its binding partners, or structurally perturb others [55]. Many FN domains were shown to act as mechanochemical switches: when FN fibers are mechanically stretched or relaxed, this can either destroy or open up binding epitopes, thereby altering the protein’s biochemical functions and changing downstream outside-in cell signaling [55–63]. Intriguingly, we have previously demonstrated that the gelatin binding domain (GBD) of FN, located on the FN₁₆FN₁₁_{1–2}FN_{17–9} region, which also overlaps with the main binding site of TG2 on FN (Fig. 1C), acts as such a mechanochemical switch in FN interactions with collagen I [61]. Thus, we asked here whether changes in the tensional state of FN fibers and their force-induced mechanical stretching and unfolding might also have an impact, or possibly regulate the binding of TG2 to FN.

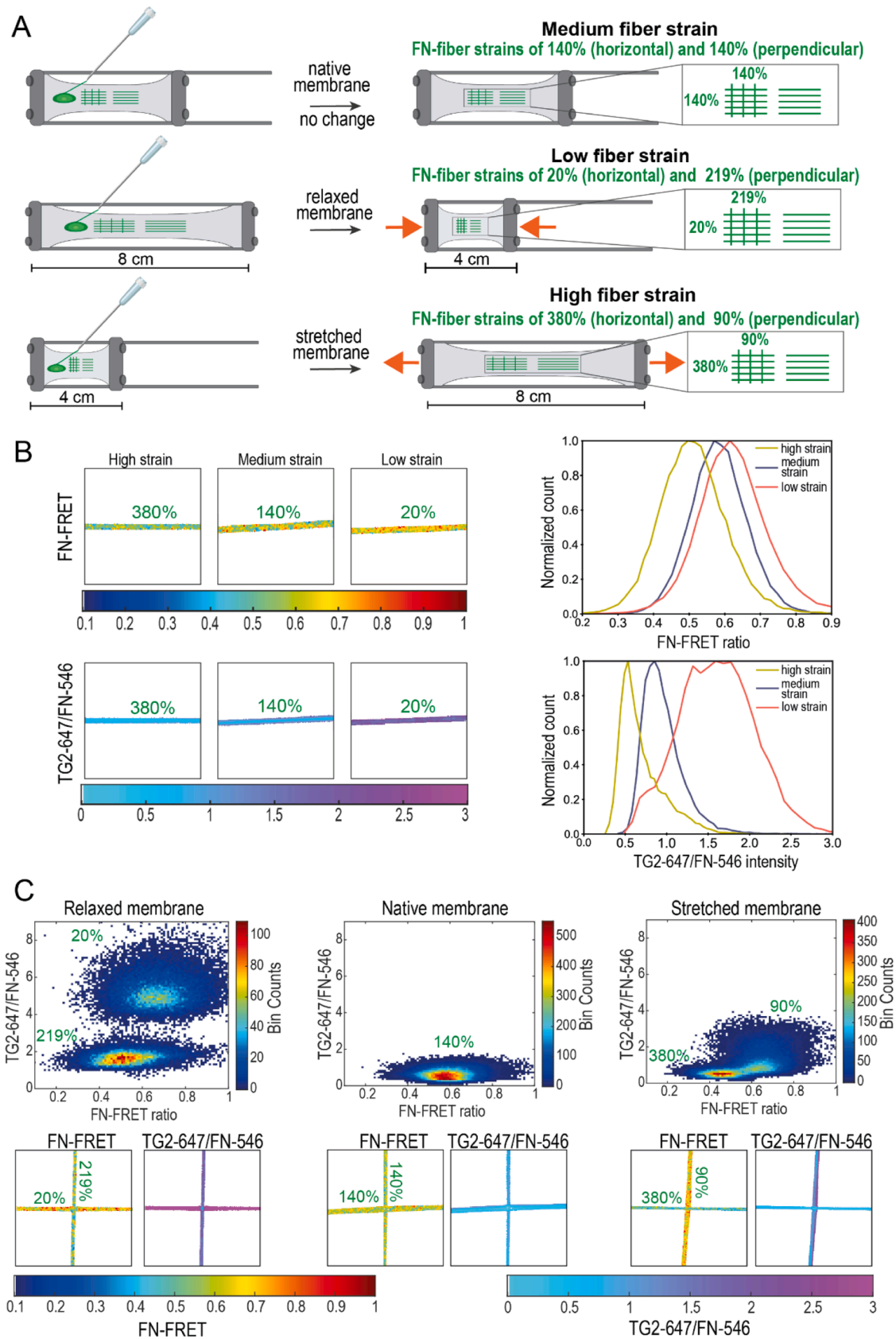
To explore the impact of FN fiber tension on TG2 affinity, we employed an in vitro FN fiber stretch assay, which enables control over the mechanical strain of FN fibers. Even though this stretch assay can be viewed as a reductionist method, FN fiber extension can be precisely controlled. We found that TG2 preferentially binds to FN fibers at low strain and displays reduced affinity when FN fibers are mechanically stretched. This mechano-regulation depends on the spatial proximity of TG2’s C-terminal β -barrel domains with the N-terminal β -sandwich. TG2 lacking β -barrel domains or TG2 in the open conformation showed no mechano-regulation, indicating that an additional synergy site for FN on C-terminal β -barrels is required for mechano-regulation. Crosslinking mass spectrometry experiments confirmed the interaction of TG2’s C-terminal β -barrels with regions outside of the canonical gelatin binding domain, specifically with FN₁₂ and FN_{III14–15}. Structural modeling corroborated these findings, suggesting multivalent synergy binding sites when TG2’s N- and C-terminal domains are in spatial proximity. We validated this model with the collagen-mimicking peptide R1R2, which competes with TG2 for FN fiber binding under different strain conditions. This study reveals insights into TG2’s interactions with fibrillar and soluble FN, shedding light on mechano-regulation in the ECM. Proteomics data are available via ProteomeXchange [64] with identifier

PXD043976 and integrative modelling structures are available via PDB-Dev [65].

Results

Mechanical stretching of FN fibers reduces their affinity for TG2 bound to GDP

To mimic the high content of fibrillar FN in the extracellular environment more closely, we employed a well-established in vitro FN fiber stretch assay in combination with a Förster resonance energy transfer (FRET) nanoscale FN strain sensor, which has already allowed us to identify a number of mechano-regulated binding partners of fibrillar FN [55,59–61,63,66]. In this assay, fibers are manually pulled with a needle tip from a droplet of FN in solution and deposited onto an elastic silicone membrane mounted on a custom-made stretch-device [59]. FN fibers were pulled and deposited either only parallel to the stretch axis, or both parallel and perpendicular to the stretch axis (Fig. 2A). By adjusting the strain of the silicone membrane, FN fibers can be either stretched or relaxed. In this study, FN fiber tension along the stretch axis of relaxed, native (silicone membrane strain unchanged), and stretched membranes is referred to as low strain (~20%), medium strain (~140%) and high strain (~380%) respectively, as calibrated previously [67]. Though the native membrane is not subjected to any strain, FN fibers are typically pre-stained to ~140% due to the forces required to pull them out of the droplet [67]. To provide a direct readout of the conformational distribution within FN fibers, FN dimers were labeled with multiple FRET donors (AF488) and acceptors (AF546) [68,69], and to avoid inter-molecular FRET, fibers always contained only 10% of FRET-labeled FN [51]. Due to mechanical stretching, the average distance between the donors and acceptors increases, therefore higher FN fiber tension corresponds to lower FRET ratios, while more relaxed FN fibers correspond to higher FRET ratios [51,69]. We controlled the responsiveness of our FN-FRET strain sensors after labeling by chemical denaturation with progressively increasing concentrations of guanidine hydrochloride (Gdn HCl) using well established protocols [51,63,69], and observed that, as expected, the FN-FRET ratios decreased as the denaturant caused FN to transition from compact to extended and then partially unfolded conformations in solution (Supplementary Fig. 2). Next, deposited FN fibers were incubated with Alexa-647 labeled TG2 (TG2-647), and the binding was assessed by measuring the TG2-647 fluorescence intensity, normalizing it pixel-by-pixel to the directly excited FN-FRET acceptor (TG2-647/FN-546), as described previously [63]. We color-coded pixel-by-pixel FN-FRET ratios within FN fibrils at each externally adjusted strain, to illustrate that FN displays a range of conformations, as also observed in the ECM fibrils assembled by fibroblasts [59,68] (Fig. 2B). As expected, the shift toward higher FN-FRET ratios was observed on the relaxed membrane and toward lower FN-FRET ratios on the stretched membrane. Histograms of the distribution of all FN-FRET pixels from a representative fiber showed that higher FN-FRET ratios corresponded to low strain, and that the highest TG2-647/FN-546 ratios were observed on the fiber experiencing low strain (Fig. 2B). To view in one image how TG2 binding affinity changes with FN fiber strain, we added human recombinant TG2 (hrTG2) to FN fibers deposited as intersections and incubated in the presence of 1 mM GDP and 1 mM EDTA. We plotted all FN-FRET pixels vs TG2-647/FN-546 pixels from the same intersection as binned scatterplots (Fig. 2C). When the strain of fibers parallel and perpendicular to the stretch axes was different (stretched membrane and relaxed membrane), FN-FRET vs TG2-647/FN-546 pixels were segregated into two separate groups with higher TG2-647/FN-546 ratios correlating with higher FN-FRET ratios. However, when the strain along both axes was the same (native membrane), pixels remained clustered as a single group (Fig. 2C). This demonstrates that TG2 binding affinity to FN is dependent on FN fiber strain. We repeated this experiment using guinea pig liver TG2 (gpTG2), which should contain all PTMs that recombinantly



(caption on next page)

Fig. 2. TG2 preferentially co-localizes with FN fibers under low strain, as revealed by the FN fiber stretch assay. A: A schematic view of the FN fiber stretch assay and the experimental setup. FN fibers were manually pulled with a needle from a droplet of concentrated FN and deposited onto a silicone membrane mounted on the custom-made stretch device. FN fibers were pulled in two ways, either only parallel to the stretch axis, or both parallel and perpendicular as intersections. Membrane was left unchanged (native), relaxed from a pre-strained position (relaxed), or stretched. Previous calibration studies converted the silicone membrane strain to the corresponding FN fiber strain [67] and are indicated on the cartoon. In this study, FN fiber strains along the stretch axis of relaxed, native, and stretched membranes are referred to as low strain (20%), medium strain (140%) and high strain (380%) respectively. Human recombinant TG2 (hrTG2) labeled with an Alexa Fluorophore 647 (TG2-647) was added to the deposited FN fibers and incubated in the presence of various effectors that are known to change its conformational state. B: On the left: Panels show a representative horizontal FN fiber for low, medium, and high strain with pixel-by-pixel color-coded FRET ratios and normalized TG2-647/FN-546 intensities. In the presence of 1 mM GDP and 1 mM EDTA, wild type hrTG2 has higher binding affinity (color-coded magenta) to the FN fiber under low strain (20%). On the right: Distributions of all FRET ratio pixels and normalized TG2-647/FN-546 from each representative fiber shown in the panels on the left were plotted as histograms. Higher FRET ratios (low strain) in the FN fiber corresponds to the higher TG2-647/FN-546 signal. C: When FN fibers are deposited as intersections, fibers along perpendicular and parallel axes are under different strains following membrane relaxation or stretching. TG2 preferentially binds the fibers under low strain (higher FN-FRET ratios). All FN-FRET ratios and TG2-647/FN-546 pixels from the same intersection were plotted as binned scatterplots. When the strain of intersecting fibers was different (relaxed and stretched membranes), plotted pixels segregated into two separate groups with higher TG2-647/FN-546 values corresponding to higher FN-FRET ratios (low FN fiber strain). When the strain of the intersecting fibers was the same (native membrane) plotted pixels remained clustered together as a single group.

produced TG2 might lack, thus confirming the reproducibility and consistency of this result (Supplementary Fig. 4).

Fifteen horizontal FN fibers deposited parallel to the stretch axis were analyzed on either native, relaxed or stretched membranes (Fig. 3A). When we incubated FN fibers with GDP-bound TG2 (TG2_{GDP}), it preferentially bound to FN fibers under low strain (~20%). TG2_{GDP} binding to FN fibers under medium (~140%) or high strain (~380%) decreased significantly, compared to the low strain. In the past we have demonstrated that stretching of FN fibers may increase non-specific binding of proteins due to higher exposure of hydrophobic residues as a result of stretch-induced partial protein unfolding [70]. However, we find that the binding affinity of TG2_{GDP} was significantly reduced by mechanical stretching of FN fibers, which suggests that specific TG2 binding sites on FN had been being destroyed. To the best of our knowledge, these findings demonstrate for the first time that TG2 binding to FN is regulated by the FN fiber tension, and that TG2 binding to FN can be weakened when FN fibers are mechanically stretched.

Spatial proximity between TG2's N-terminal domain and the C-terminal β -barrels is required for its mechano-regulated binding to FN

Since an earlier study suggested that formation of the TG2-FN complex is not altered by the presence of TG2 effectors [44], we were surprised to find that the mechano-regulated binding was abolished upon addition of saturating amounts of Ca²⁺ (10 mM) (Fig. 3B and Supplementary Fig. 6A). In the presence of Ca²⁺, we no longer detected TG2's high affinity binding towards FN fibers under low strain. Instead, calcium bound TG2 (open state) showed the same, low level of binding towards FN fibers at all strains. A more detailed analysis revealed a dose-dependent reduction of TG2 binding to FN fibers under low strain upon titration with increasing amounts of calcium (Supplementary Fig. 7). Interestingly, there was no significant difference in TG2 binding to FN fibers under conditions of high strain (380%) compared to medium strain (140%) (Fig. 3A). The likely explanation for this observation is that the forces within the μ N range required to pull FN fibers from the FN solution are already sufficient to mechanically stretch and disrupt the majority of TG2 binding sites on FN [67]. Since there was no significant difference in TG2 binding to FN fibers under medium strain (140%) and high strain (20%), the medium strain condition in the next set of experiments was not included.

Most of the TG2 in the ECM is thought to be reversibly inactivated due to the allosteric disulfide bond formation which locks the enzyme in the extended open state [40,71]. A similar conformation is induced by some active-site irreversible TG2 inhibitors, such as the active site-specific inhibitor Z006 (Z-DON-Val-Pro-Leu-OME, "Z-DON") [37, 41] (Fig. 1B). Therefore, we also investigated the binding of oxidized TG2 (oxTG2) and inhibitor Z006 bound TG2 (TG2_{Z006}), in comparison to TG2_{GDP}. (Fig. 3D-F and Supplementary Fig. 8). To prepare oxTG2 and TG2_{Z006}, WT gpTG2 was incubated for 3 h at 37°C with 2 mM oxidized

glutathione (GSSG) and 1 mM EDTA, or for 1 h at room temperature with 100 μ M Z006 and 1.2 mM CaCl₂. As before, WT TG2_{GDP} preferentially bound to FN fibers under low strain (Fig. 3D). In contrast, both oxTG2 and TG2_{Z006} bound FN equally, regardless of the FN fiber strain (Fig. 3E, F and Supplementary Fig. 8). Since this behavior was not anticipated based on previous studies using soluble FN [44], we next looked for a testable structural hypothesis how TG2 binding to FN could be mechano-regulated. Cardoso *et al.* have mapped the FN binding site on TG2 to a region on the N-terminal domain [44], as indicated in Fig. 1A. Inspection of the structure suggests that the second β -barrel in TG2's closed state is in proximity to the proposed FN binding site (Fig. 1A). The "beads-on-a-string" like structure of FN (Fig. 1C) suggests that adjacent FN modules could possibly form synergistic contacts, thereby stabilizing the TG2-FN complex on low tension FN fibers. In contrast, when TG2 is in the extended open state, the second β -barrel is out of reach and no additional contacts could be formed. To test whether β -barrels of TG2 participate in the mechano-regulated binding to FN fibers, we have used a short TG2 variant (1-465aa, β -barrel 1 and 2 deleted) in our FN fiber stretch assay. Indeed, short TG2 showed the same behavior as calcium activated WT TG2, oxTG2 and TG2_{Z006} and exhibited no mechano-regulated binding to FN fibers (Fig. 3C and Supplementary Fig. 6B). This suggests that for the mechano-regulated binding, the β -barrels of TG2 need to be present and must be in spatial proximity to the N-terminal domain. Interestingly, there was no significant difference in binding between oxTG2 and TG2_{Z006} to FN fibers under high strain (~380%), however TG2_{GDP} binding affinity was significantly higher compared to oxTG2 and TG2_{Z006} on high strain FN fibers (Supplementary Fig. 8C). Upon mechanical stretching of FN fibers, a large distribution of conformational FN states exists within each FN fiber that upon stretching gets gradually more shifted towards partially unfolded states [67,72]. Thus, the ensemble of specific binding sites on FN gets gradually destroyed by fiber stretching, not at one specific strain. This is due to the non-periodic bundling of FN molecules within the fibers, which interferes with the mechanical hierarchy in which FN domains would get unfolded in isolated molecules [72]. Consequently, the specific TG2-binding sites on FN are being destroyed gradually with increasing FN fiber strain, as observed previously for other binding partners [51,59,61,63,67]. Thus, FN fiber stretching results in a progressive reduction of TG2_{GDP} binding. However, since the N-terminal domain and C-terminal β -barrels of TG2_{GDP} are in spatial proximity, unlike in oxTG2 and TG2_{Z006}, TG2_{GDP} can maintain additional contacts to the remaining intact binding sites on FN. Thus, this result also agrees with our hypothesis.

Catalytic activity of TG2 has no effect on the loss of mechano-regulated binding to fibrillar FN

To ensure that the loss of the mechano-regulated binding of TG2 to FN fibers in the presence of calcium was not due to TG2 crosslinking

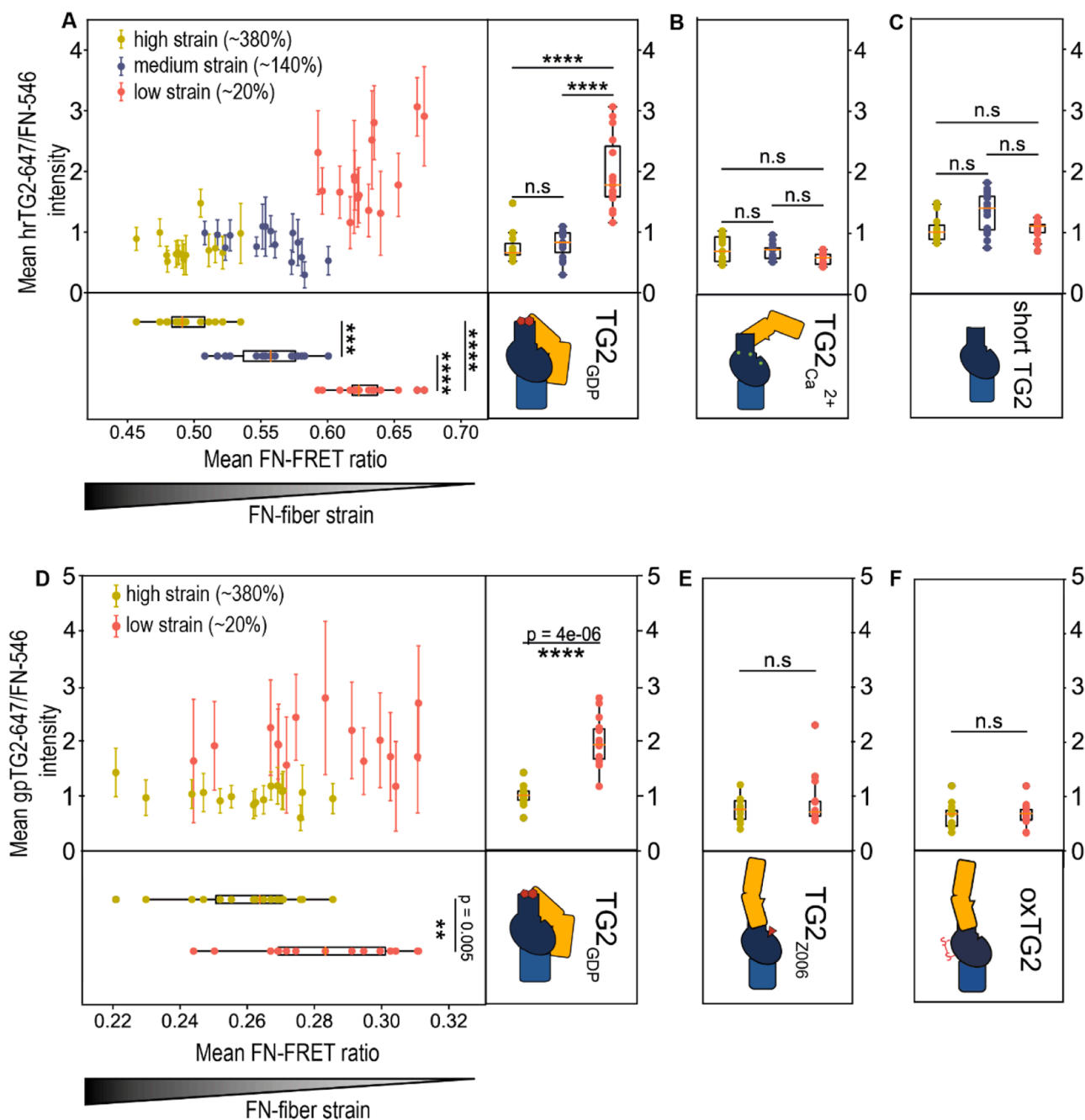


Fig. 3. FN fiber stretch assay data showing the dependence of mechano-regulated TG2-FN binding on TG2's conformational states and its C-terminal β -barrels comparing human recombinant and guinea pig liver TG2 (hrTG2 and gpTG2). The mean of the distribution of FN-FRET ratios from all pixels of one fiber was plotted against the mean of the distribution of the normalized TG2-647/FN-546 intensity. 15 fibers were analyzed per membrane strain (Full data sets: Supplementary Fig. 6 & 8). A: Human recombinant TG2 (hrTG2) has a higher binding affinity toward FN fibers under low strain ($\sim 20\%$) in the presence of 1 mM GDP and 1 mM EDTA, which induce a closed TG2 conformation. B: hrTG2 binds FN with equal affinity in the presence of 10 mM Ca^{2+} which induces an open TG2 conformation regardless of FN fiber strain. C: Short TG2 (β -barrels 1 and 2 are deleted) binds FN with equal affinity regardless of FN fiber strain. Short TG2 was labelled separately from hrTG2 and has a different degree of labelling, therefore its fluorescent intensity should not be compared to $\text{TG2}_{\text{Ca}^{2+}}$ or TG2_{GDP} . D: Like hrTG2 in (A), guinea pig liver TG2 (gpTG2), preferentially bound with higher affinity to FN fibers under low strain ($\sim 20\%$) in the presence of 1 mM GDP and 1 mM EDTA (closed-state TG2). When gpTG2 was incubated with the irreversible active-site inhibitor Z006 (Z-DON) (E) or oxidised with GSSG (F), both of which induce an extended open-state TG2 conformation, TG2_{Z006} and oxTG2 bound FN equally, regardless of FN fiber strain. Statistical significance was computed with Wilcoxon rank-sum statistic for two samples. p -values: ($*0.01 \leq p < 0.05$; $**0.001 \leq p < 0.01$; $***10^{-5} \leq p < 0.001$; $****10^{-6} \leq p < 10^{-5}$; $***** p < 10^{-6}$).

activity or TG2 self-crosslinking [73], we conducted a control experiment using an inactive Cys277Ser-TG2 mutant (Supplementary Fig. 9). TG2 is stabilized in the closed conformation by an H-bond between Cys277 (catalytic core) and Tyr516 (β -barrel 1) [74]. Cys277Ala/Ser-TG2 mutants which are less efficient in forming this H-bond, are known to predominantly assume an open conformation. We observed

that in the presence of 1.2 mM calcium, the Cys277Ser-TG2 mutant bound FN fibers at both high ($\sim 380\%$) and low ($\sim 20\%$) strains equally well, indicating that it is indeed the open conformation of TG2 that abolishes mechano-regulated binding to FN fibers, and not its cross-linking activity. Addition of 1 mM GDP increased the Cys277Ser-TG2 binding affinity to FN fibers at low strain ($\sim 20\%$); however, the

significance level of this increase was considerably less ($p = 0.004$) compared to the wild type hrTG2 ($p < 10^{-5}$). Cys277/Ala/Ser-TG2 mutants are less efficient in binding GDP and tend to assume the open conformation [74], thus explaining the reduced significance level of the observed increase as well. All these results confirm that the conformational state and not the crosslinking activity of the open-state TG2 plays the central role in the loss of the mechano-regulated binding to FN fibers.

TG2's affinity to surface-adsorbed FN depends on its conformation and the C-terminal β -barrel domains

While previous studies suggested that TG2 binding to surface-adsorbed FN is independent of TG2's conformation and C-terminal domains [44], our conclusions drawn from FN fiber stretch assays supported the opposite. To investigate if the distinct conformational states of fibrillar FN versus surface-adsorbed FN played a role, we repeated the experiments using the latter.

We coated microtiter plates with human plasma FN or the 45-kDa FN gelatin-binding domain (GBD) at concentrations from 1 $\mu\text{g/ml}$ to 50 $\mu\text{g/ml}$. FN was detected using a specific monoclonal antibody and the fluorescence intensity was measured. The optimal FN concentration for coating was determined at 2.2 $\mu\text{g/ml}$ for full-length FN (Fig. 4A). To ensure a similar number of TG2 binding sites as with full-length FN, we determined that 0.6 $\mu\text{g/ml}$ of the GBD was suitable for plate coating (Fig. 4B). We then evaluated TG2 binding to surface-adsorbed FN under different conditions. Surprisingly, TG2 exhibited varying affinities for adsorbed FN depending on its conformational state induced by specific TG2 effectors: $\text{TG2}_{\text{CaCl}_2} < \text{TG2}_{\text{EDTA}} < \text{TG2}_{\text{GDP}} < \text{TG2}_{\text{Z006}}$ (Fig. 4C). In contrast, short TG2 (1-465aa, β -barrel 1 and 2 deleted) exhibited consistent binding affinities across conditions (Fig. 4D).

Additionally, TG2 had a higher binding affinity for full-length FN, likely due to additional contacts outside the GBD (Fig. 4E). These findings highlight that TG2's affinity for surface-adsorbed FN is modulated by its conformational state as influenced by allosteric effectors. Moreover, the C-terminal domains of TG2 play a crucial role in enhancing binding to surface-adsorbed FN, increasing TG2's interactions with both fibrillar and surface-adsorbed FN.

C-terminal β -barrels of TG2_{GDP} interact with regions outside the canonical gelatin-binding domain (GBD) of FN in solution

As the short form of TG2 without β -barrel domains no longer exhibited sensitivity to the FN fiber strain, and bound both stretched and relaxed FN fibers equally, this implies the presence of a secondary FN binding site on the C-terminal β -barrel domains of TG2. Yet, no information was available in the literature about the role of these domains in TG2's interaction with FN. To explore the possibility of multivalent synergy binding sites, we used crosslinking mass spectrometry [75] (XL-MS) to map contact sites between the two proteins. XL-MS uses chemical reagents to induce covalent bonds between spatially proximal amino acids within or between proteins. Crosslinking sites are identified after enzymatic digestion of crosslinked proteins and sequencing of the resulting connected peptide pairs by mass spectrometry. Previous studies employing similar proteomic approaches (hydrogen-deuterium exchange - HDX) using only FN's GBD in complex with TG2_{Z006} , did not identify any regions on the C-terminal β -barrel domains of TG2 that could interact with FN [44]. This is in agreement with our hypothesis, as the inhibitor Z006 is known to trap TG2 in the extended open conformation, which spatially separates the C-terminal domains from the N-terminal domain, making them inaccessible to FN [37]. To our knowledge, interacting regions of TG2_{GDP} (closed state) and full-length FN have not been mapped with either approach. Thus, we performed for the first time XL-MS analysis of TG2_{GDP} in complex with full-length FN, and of TG2_{GDP} in complex with the FN's GBD, to better compare our findings with the available literature.

Among the resulting FN isoforms, we were able to unequivocally identify FN isoform 1, which was used for the subsequent data analyses. Validated crosslinks were displayed on circular diagrams with the help of xVis [76] (Fig. 5 and Supplementary Fig. 10–11). In total, 20 unique crosslinks were identified between TG2_{GDP} and FN, or TG2_{GDP} and GBD complexes (Supplementary Note 2 and Fig. 5). Remarkably, the C-terminal β -barrel 2 was in close contact with FNIII_{14–15} (4 unique inter-protein crosslinks), as well as with FNI₂ (3 inter-protein crosslinks). Simultaneously, FNIII_{14–15} and FNI₂ were in close contact with each other, as indicated by multiple intra-protein crosslinks between those regions (magenta lines in Fig. 5). From experiments with the TG2 and GBD and chymotrypsin as a protease, 8 additional unique inter-protein crosslinks were detected (Supplementary Fig. 11). Notably, we identified a crosslink between Lys30 (TG2) and Lys486 (GBD, numbering for full length FN). TG2 residue Lys30 is known to be one of the three residues (Lys30, Arg116, His134) that comprise the main FN-binding site on the N-terminal β -sandwich of TG2 [44]. Interestingly, the crosslink involving Lys486 was not found when TG2 was in complex with the full-length FN (Supplementary Note 2 and Supplementary Fig. 10). Instead, Lys30 on TG2 was crosslinked to Lys1837 and Lys1862 on FNIII₁₄. This difference could arise from the variations in reactivity between these lysine residues and structural differences. These MS data clearly demonstrate that the C-terminal domains of TG2 interact with regions of FN outside of the canonical GBD when FN is in a compact quaternary conformation in solution, and when the C-terminal β -barrels are in spatial proximity to the N-terminal domain.

Crosslink-guided structural modelling of TG2 and FN

XL-MS not only identifies which regions of a protein complex are in close contact, but also provides valuable spatial information through physical distance restraints imposed by each crosslinker. The spatial information can be used for modelling and docking to determine the position and orientation of proteins within a complex [77]. To determine the binding interface of the TG2-FN complex using low-resolution restraint data more accurately, we integrated the experimental crosslinks into a modelling pipeline [78,79] (Supplementary Fig. 13). We selected a few regions of FN for modelling based on criteria such as the availability of templates in PDB, coverage by crosslinks, and existing knowledge in the literature regarding binding sites. The regions that met these criteria and were suitable for structural modelling were FNI_{2–3}, FNI_{7–9}, FNI₆FNII_{1–2} FNI_{7–9} (GBD), and FNIII_{14–15} (Supplementary Note 1). To build crosslink-guided models, we used the I-TASSER [80] and submitted experimental intra-protein crosslinks as distance restraints to structurally refine the available crystal structure templates, as was previously done [78]. To evaluate the compatibility of refined models with experimental restraints, we calculated Euclidean distances (ED) between β -carbons (CB-CB) of crosslinked residues using Xwalk [81]. We classified crosslinks into compatible and non-compatible based on the distance cut-off values [78,82]: ED for DSS < 35 Å, ED for DMTMM < 25 Å, ED for PDH < 35 Å.

We identified 4 intra- and 3 inter-protein crosslinks for FNI_{2–3}. A high-resolution crystal structure of FNI_{2–3} was available (PDB:2cg7), which we submitted as a template to I-TASSER for structural refinement with experimental crosslinks. After structural refinement, a high scoring model was selected, that satisfied all crosslinks within the distance cut-off (Supplementary Note 1). For FN's GBD, we detected 3 intra- and 8 inter-protein crosslinks. Templates covering FNI₆FNII_{1–2}FNI₇ and FNI_{8–9} domains, except for the short linker (513–516aa) between them, were available as PDB:3mql and PDB:3ejh, respectively. However, our initial attempt to model the entire GBD with I-TASSER was not satisfactory. Thus we used ROBETTA [83] and AlphaFold [84] to determine the orientation of FNI₆FNII_{1–2}FNI₇ and FNI_{8–9} with respect to each other. To evaluate the quality of predicted models of GBD, we submitted them to QMEAN [85], which evaluates how the model performs in comparison to the experimental PDB structures. The AlphaFold predicted that the

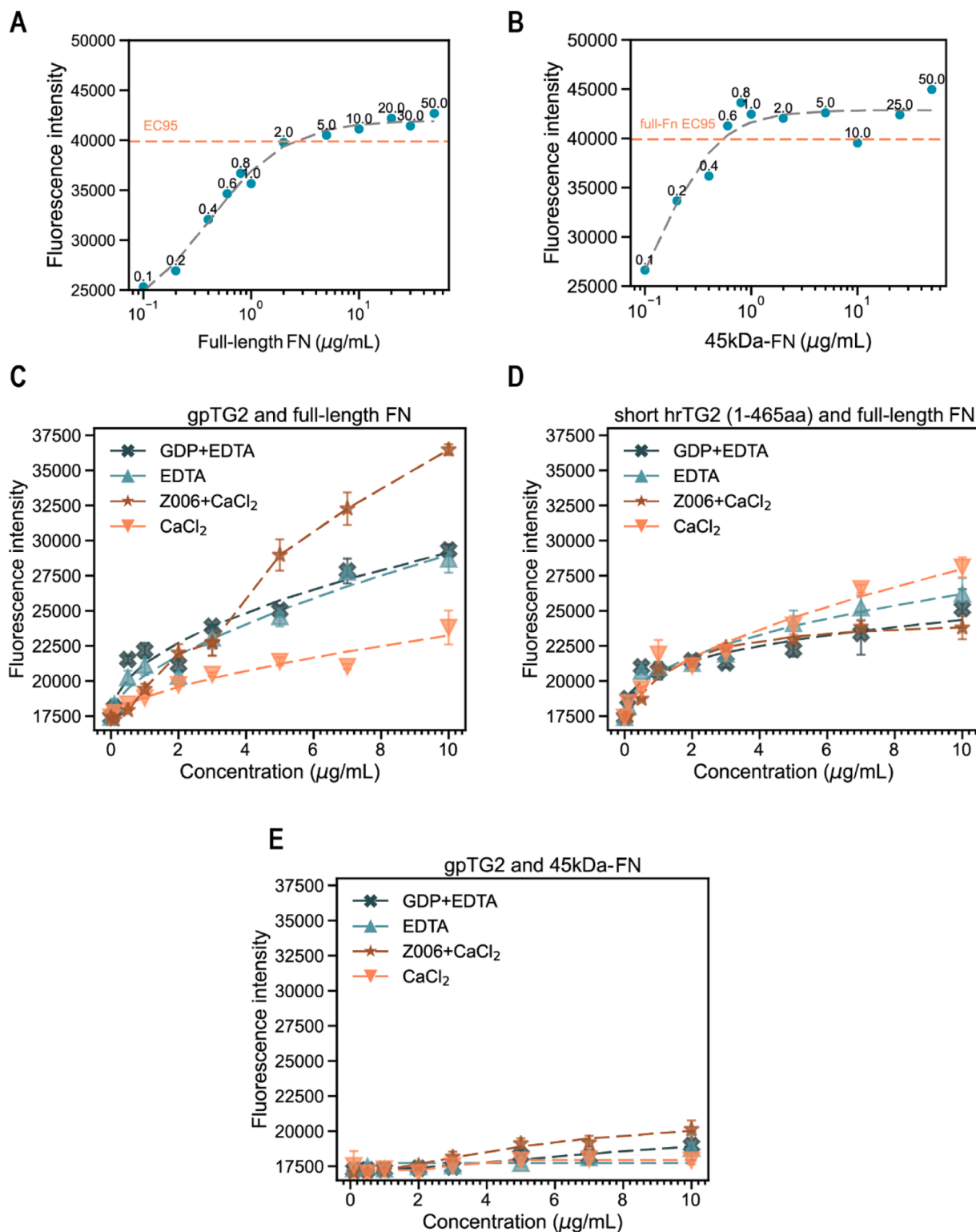


Fig. 4. Microplate protein-binding assay data with TG2 binding to surface-adsorbed full-length FN, or to FN's 45 kDa gelatin binding domain (GBD). A: 96-well microplates were coated with concentration series of full-length FN at 4°C overnight. FN was detected with a monoclonal anti-FN antibody with an epitope within the gelatin binding domain (GBD). From the fitted curve, the maximal fluorescent intensity was determined at a concentration of 2.4 $\mu\text{g/ml}$ of full-length FN 95%. B: 96-well microplates were coated with concentration series of 45 kDa-FN GBD at 4°C overnight and detected using the same anti-FN antibody as in (A). From the fitted curve, the maximal fluorescent intensity observed for the full-length FN was determined at 0.6 $\mu\text{g/ml}$ of 45 kDa-FN GBD 95%, and this concentration therefore corresponds to the same approximate number of TG2 binding sites on 45 kDa-FN GBD. C: Binding affinity of wild type guinea pig TG2 (WT gpTG2) to the surface-adsorbed FN changes depending on the presence of GDP, Ca²⁺ and Z006 TG2 effectors. D: Deletion of TG2's β -barrels 1 and 2 results in indiscriminate binding affinity of short TG2 mutant to adsorbed FN, regardless of the presence of GDP, Ca²⁺ and Z006 effectors. E: When plates were coated with 0.6 $\mu\text{g/ml}$ of FN's 45 kDa-FN fragment, which corresponds to the same number of binding sites as when coated with 2.4 $\mu\text{g/ml}$ full-length FN, WT gpTG2 had drastically reduced binding affinity toward 45 kDa-FN fragment. *For the coatings of microtiter plates, 2.4 $\mu\text{g/ml}$ of full-length FN and 0.6 $\mu\text{g/ml}$ of 45 kDa-FN were used, which approximately correspond to the same number of binding sites for TG2, as was determined by the titration experiments in A and B.

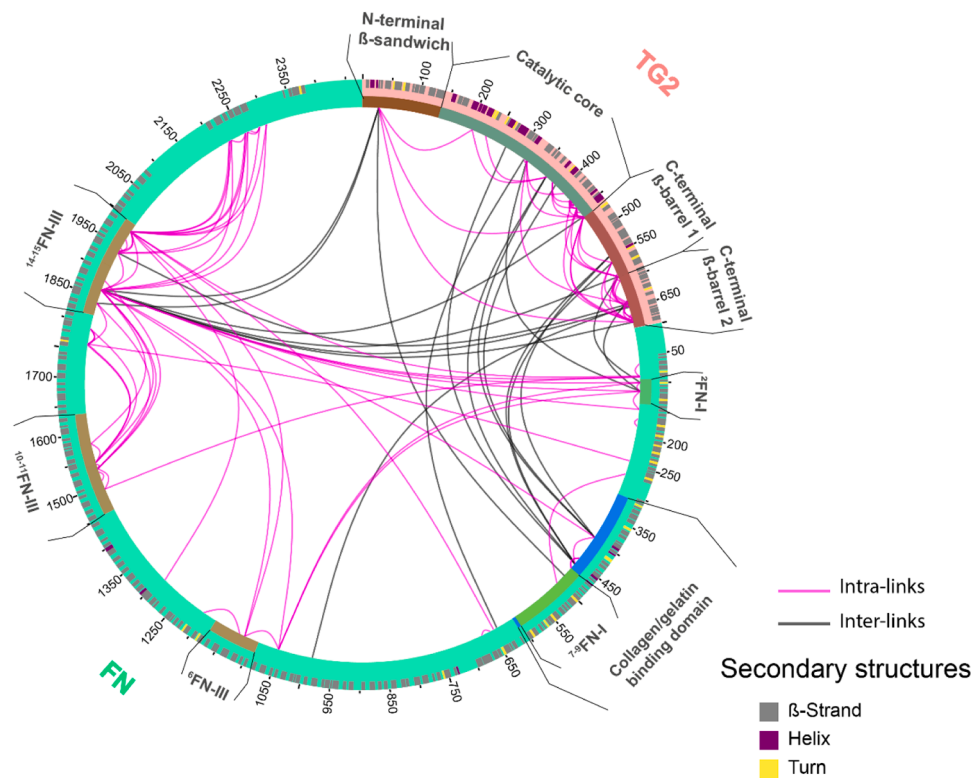


Fig. 5. Cross-links identified with the XL-MS of the TG2_{GDP} and FN complex reveal that TG2's C-terminal β -barrel domains interact with regions outside of the canonical GBD. A: Circular diagram simultaneously shows a population of 20 unique inter-protein crosslinks identified from both TG2-FN and TG2-45 kDa-FN complexes using trypsin and chymotrypsin as proteases. To view them separately, go to Supplementary Fig. 10–11. Crosslinks only within TG2 or only within FN (intra-protein crosslinks) are shown in magenta, crosslinks between TG2 and FN (inter-protein crosslinks) are shown in black. C-terminal β -barrel 2 of TG2_{GDP} is in close contact with FNIII_{14–15} (Lys1862 and Lys1936) and FNII₂ (Lys100 and Lys116). Simultaneously, FNIII_{14–15} and FNII₂ are in proximity to each other, as shown by magenta intra-protein crosslinks. TG2 residue Lys30, which is one of the three residues (Lys30, Arg116, His134) comprising the main FN-binding site on the N-terminal β -sandwich [44], was crosslinked to Lys486 (45 kDa-FN, numbering for full-length FN). On the full-length FN, Lys30 was crosslinked to residues Lys1837 (FNIII₁₄) and Lys1862 (FNIII₁₄). Visualization performed using xVis Webservice [76].

GBD model outperformed the ROBETTA model (QMEAN Z-score=1.44 vs 1.86). This indicates better compatibility of the structural model predicted by AlphaFold than ROBETTA with the experimentally determined crosslinks. Consequently, we selected the AlphaFold predicted model of GBD for docking with HADDOCK [86].

Although we detected only one inter-protein crosslink and no intra-protein crosslinks for the FN_{7–9} domains, we included it in the modeling pipeline. FN_{7–9} is well-known to be the high affinity binding region for TG2 and behaves as the whole 45-kDa GBD in mediating cell functions such as adhesion, spreading and migration [45]. To model FN_{7–9}, we followed the same strategy we used for the GBD. The AlphaFold predicted model of FN_{7–9} deviated less than one standard deviation from the experimental structures deposited in the PDB (QMEAN Z-score=0.64), whereas the ROBETTA predicted model deviated by two standard deviations (QMEAN Z-score=2.02). Therefore, we selected the AlphaFold predicted model of FN_{7–9} for further docking steps, given its overall better performance (Supplementary Note 1).

We identified 11 intra- and 7 inter-protein crosslinks for FNIII_{14–15} and submitted the high-resolution crystal structure of FNIII_{14–15} (PDB:1fnh) along with crosslinks for structural refinement using I-TASSER. A high scoring model that satisfied 10/11 intra-protein crosslinks was selected. The non-compatible crosslink (Lys1862-Lys1936) connects two interdomain residues located on FNIII₁₄ and FNIII₁₅. As these two domains are connected by a flexible linker, it is expected that structural rearrangements favouring a more closed conformation might occur.

For TG2, we detected 46 intra-protein crosslinks, 8 of which violated distance cut-off when we mapped them on the model. All the non-compatible crosslinks were between the interdomain residues.

Specifically, 5 non-compatible crosslinks were between residues on the catalytic core and C-terminal domain, 2 between residues on C-terminal domains, and 1 between N-terminal domain and the catalytic core (Supplementary Note 1). As these domains are connected by flexible linkers, non-compatible residues suggest that TG2 undergoes some structural rearrangement upon binding to FN in solution. After performing structural refinement, one notable improvement was residue Lys30, which on the available TG2 template (PDB:4pyg) did not comply with our solvent accessibility criteria (Supplementary Note 1). The Lys30 residue was previously shown by mutagenesis studies to be crucial for FN-binding [44]. After recalculation of TG2 template using experimental intra-protein crosslinks, all three residues comprising the high-affinity FN-binding site (Lys30, Arg116, His134) satisfied the solvent accessibility criteria. Overall, by integrating experimental crosslinks as distance restraints, we were able to structurally refine available templates to be in better agreement with the experimental MS data.

Crosslink-guided HADDOCK docking of TG2 with FN_{7–9} revealed a parallel alignment of FN modules with TG2's C-terminal β -barrels

Protein complexes in solution are typically dynamic, and crosslinks can reflect an averaged ensemble of conformations. However, non-compatible crosslinks that may belong to an alternative complex conformation can negatively impact the accuracy of the docking results. To address this issue, we utilized the DisVis webserver, which filters out non-compatible crosslinks and predicts key residues involved in binding at the interaction interface using experimental crosslinks [87]. Our analysis using DisVis highlighted three putative incompatible crosslinks, namely the Lys319(TG2)-Glu116(FN) crosslink between TG2 and

FNI₂₋₃, the Lys550(TG2)-Lys397(FN) crosslink between TG2 and GBD, and the Lys464(TG2)-Lys1862(FN) crosslink between TG2 and FNIII₁₄₋₁₅ (Supplementary Note 2). While it is important to note that these crosslinks may not necessarily be false and are likely to belong to an alternative conformation of the complex, we did not further investigate this possibility due to insufficient number of crosslinks. Therefore, we excluded these crosslinks from further docking steps with HADDOCK to improve the accuracy of the docking results.

To identify the putative active residues at the binding interface, we filtered out the residues with less than 40% relative solvent accessibility for the backbone or side chain using NACCESS [88], and then used DisVis interaction analysis to predict active residues at the binding interface consistent with submitted experimental crosslinks (Supplementary Note 2). Active residues, along with confirmed crosslinks mutually compatible after selection by DisVis, were submitted for separate docking runs with HADDOCK for the TG2 and FNI₂₋₃, TG2 and FNI₇₋₉, TG2 and FNIII₁₄₋₁₅, TG2 and GBD complexes (Supplementary Note 3). After docking, we mapped crosslinks of predicted models and used Xwalk to calculate distances between crosslinked residues to identify any non-compatible crosslinks. The models of TG2-FNI₂₋₃ and TG2-FNIII₁₄₋₁₅ complexes satisfied all crosslinks that were submitted to guide docking, and the models with the highest HADDOCK score were selected (Fig. 6A, B). In the case of the TG2-FNI₇₋₉ complex, we guided docking by a single crosslink, which was compatible on all resulting models, thus we selected the model with the highest HADDOCK score. Notably, one of the predicted models of the TG2-FNI₇₋₉ complex supported the parallel alignment of FNI₈₋₉ with C-terminal β -barrels of TG2, while FNI₇ was aligned with the high-affinity site on the N-terminal domain of TG2 (Lys30, Arg116, His134) (Fig. 6C). This docking pose strongly supports the hypothesis of multivalent binding sites, which suggests a structural mechanism that can indeed explain the mechano-regulated TG2 binding to fibrillar FN.

Collagen-mimicking peptide R1R2 and TG2_{GDP} compete for binding to FN fibers

To better understand the results of XL-MS experiments, where we used soluble FN in a compact conformation, in relation to the results of the FN fiber stretch assay, in which FN was in fibrillar form, we sought to validate the predicted model for the TG2-FN complex. Previous studies have identified the TG2 and collagen binding sites on FN within the 45-kDa GBD [49,89]. Although both binding partners interact with several FN modules, FNI₈ appears to be particularly important for collagen as well as for TG2 binding [45,89]. Our predicted model of the TG2-FNI₇₋₉ complex suggested an overlap between TG2 and collagen-binding sites on FNI₈ within the GBD. To validate this model, we investigated whether simultaneous binding of TG2 and collagen to fibrillar FN is possible. To test this, we utilized the R1R2 collagen-mimicking peptide, which is derived from the SFS FN-binding protein of the pathogen *Streptococcus equi* [90]. Both R1R2 and collagen share a conserved GEXGE motif which has been shown by crystallography to bind to FNI₈₋₉. As a result, R1R2 inhibits binding of FN to collagen I [89,91]. We also previously demonstrated that the R1R2 binding motif on FN is destroyed by stretching FN fibers [61].

To assess the influence of collagen on TG2-FN binding, we added increasing concentrations of R1R2 peptide to 100 μ g/ml of TG2_{GDP} (1 mM GDP, 1 mM EDTA, 1 mM MgCl₂ in 50 mM Tris) and incubated the FN fibers under low strain for 1 h. This R1R2 titration series revealed a dose dependent reduction of TG2 binding to FN, indicating that R1R2 can prevent the specific interactions between TG2_{GDP} and FN fibers under low strain (Fig. 7A). Next, we tested how TG2 would bind FN fibers in the presence of 100 μ M R1R2 at all strains. Indeed, in the presence of high concentrations of R1R2, TG2 is equally bound at low levels to FN fibers at all strains (Fig. 7B). Interestingly, the addition of 100 μ M R1R2 further significantly reduced TG2_{GDP} binding to the FN fibers under high strain, indicating that TG2 and R1R2 were still competing for

the remaining specific binding sites on FN (Supplementary Fig. 12). Our findings thus confirm that the binding of TG2 to the FN fibers under high strain is still specific, but weaker as the ensemble of destroyed multi-domain binding epitopes increases by stretching FN fibers. Therefore, our data demonstrate for the first time that the collagen-mimicking peptide R1R2 and TG2 directly compete on fibrillar FN under low as well as high fiber strains.

Discussion

This study has addressed for the first time whether TG2's interaction with fibrillar FN might be regulated by the tensional state of FN fibers. Using an in vitro FN fiber stretch assay and a FN-FRET nanoscale strain sensor, we found that TG2 binds more strongly to relaxed FN fibers than to stretched FN fibers (Fig. 2). This mechano-regulated binding is dependent on the spatial proximity of TG2's C-terminal β -barrels to its N-terminal domain, as demonstrated by experiments involving C-terminal β -barrel deletions, calcium, inhibition with Z-DON, and oxidation (Fig. 3). Importantly, we also confirmed that TG2's mechano-regulated FN binding does not require its catalytic activity, but is dependent on its conformations, as shown with the Cys277Ser TG2 inactive mutant (Supplementary Fig. 9). Notably, TG2's binding affinity varies not only with fibrillar FN, but also with surface-adsorbed FN, which has a more compact conformation (Fig. 4). Again, TG2's conformation and the presence of its C-terminal β -barrels are critical for this binding, and TG2's binding affinity to a 45-kDa FN fragment decreased drastically compared to full-length FN (Fig. 4 C, E).

This finding is remarkable, as it contrasts with a previous study that reported TG2 binding to the GBD with the same affinity as full-length soluble FN [49]. However, the contrasting result can likely be explained by the fact that the TG2 binding between FN's GBD and full-length FN was not compared in terms of equivalent numbers of binding sites available to TG2 in that previous study. Collectively, these results indicate that the C-terminal domains of TG2 support its interaction with FN, in synergy with N-terminal domain, and that this interaction thus enhances TG2's affinity to FN beyond the known GBD interaction. This conclusion was confirmed by XL-MS, which showed that TG2's C-terminal β -barrels interact with regions of FN outside of the canonical GBD region, specifically with FNI₂ and FNIII₁₄₋₁₅ (Fig. 5). Notably, an earlier study using rotary shadowing electron microscopy reported a possible TG2 binding to FNI₄₋₅ regions alongside the conventional GBD [92]. However, subsequent studies were not able to detect this interaction, possibly due to the use of separate FN fragments as opposed to exploring a possible synergy site localization [45–47]. Our XL-MS result is highly significant, since studies that aim to develop small molecule inhibitors of TG2-FN interactions often utilize FN's 45-kDa FN fragment instead of the full-length FN [33,34]. While our XL-MS data did not definitively indicate whether TG2's C-terminal domains interact with FNI₂₋₃ and FNIII₁₄₋₁₅ simultaneously, such simultaneous interaction is suggested by spatial proximity of FNI₂₋₃ and FNIII₁₄₋₁₅, as is evident from numerous inter-protein crosslinks within FN connecting those two regions (Fig. 5).

Using XL-MS and crosslink-guided structural modeling, we have shown that TG2 residues on both N-terminal β -sandwich and C-terminal β -barrels are predicted to interact with FN, but only when TG2 adopts a closed conformation (Fig. 6). It is important to note that a compact conformation of soluble FN, which was present in our XL-MS experiments must be distinguished from fibrillar FN. When FN is in the soluble compact conformation, the FNI₂₋₃ and FNIII₁₄₋₁₅ modules are brought in spatial proximity attracted by long-range electrostatic interactions, but are spatially separated when FN assumes a fibrillar form [52]. However, since FN molecules are not periodically arranged in FN fibers, yet are closely-packed [54,72], FNI₂₋₃ and FNIII₁₄₋₁₅ modules from neighboring molecules could happen to be at the right distance. Additionally, one of the predicted docking models of TG2 with FNI₇₋₉ suggested a parallel alignment of the FNI₈₋₉ modules with the C-terminal β -barrels of TG2,

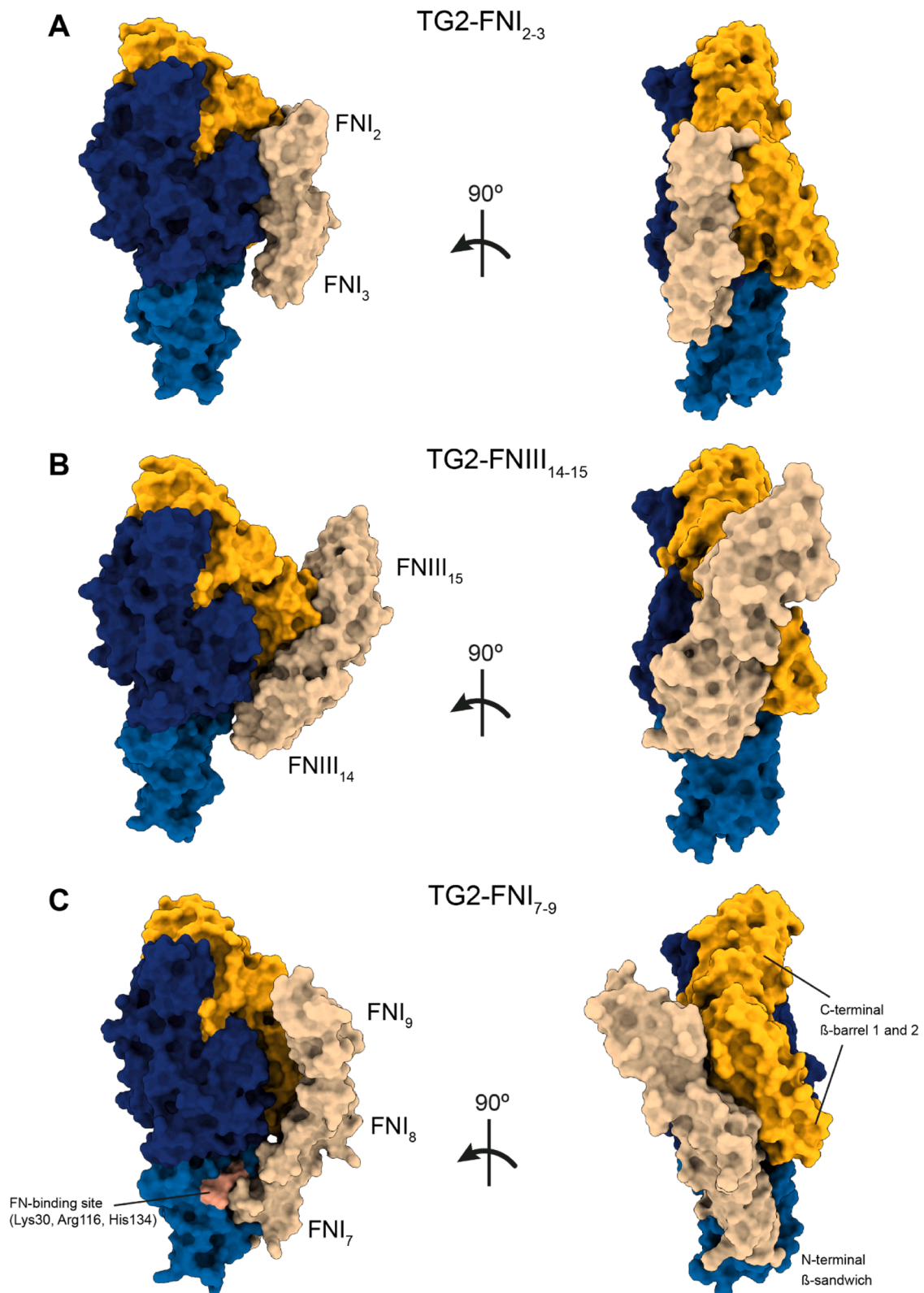


Fig. 6. Protein-protein docking with HADDOCK of TG2 complexed with selected FN fragments guided with experimental crosslinks as distance restraints. Predicted models of (A) TG2 in complex with FNI₂₋₃, (B) TG2 in complex with FNIII₁₄₋₁₅, and (C) TG2 in complex with FNI₇₋₉. The resulting docking pose of the TG2-FNI₇₋₉ complex supports parallel alignment of FNI₈₋₉ with the C-terminal β -barrels of TG2, while FNI₇ is in contact with TG2's canonical FN-binding site (Lys30, Arg116, His134, colored pink) on the N-terminal β -sandwich. Full data set with mapped crosslinks is available in Supplementary Note 3 and Supplementary Fig. 15–17.

while TG2's main FN-binding site on N-terminal domain (residues Lys30, Arg116, His134) was in contact with FNI₇ (Fig. 6C). Such an orientation also would allow for additional stabilizing contacts between

C-terminal domains and fibrillar FN and could mediate the mechano-regulated binding between TG2 and FN fibers. Therefore, it is possible that mechano-regulated TG2 binding to FN fibers is mediated

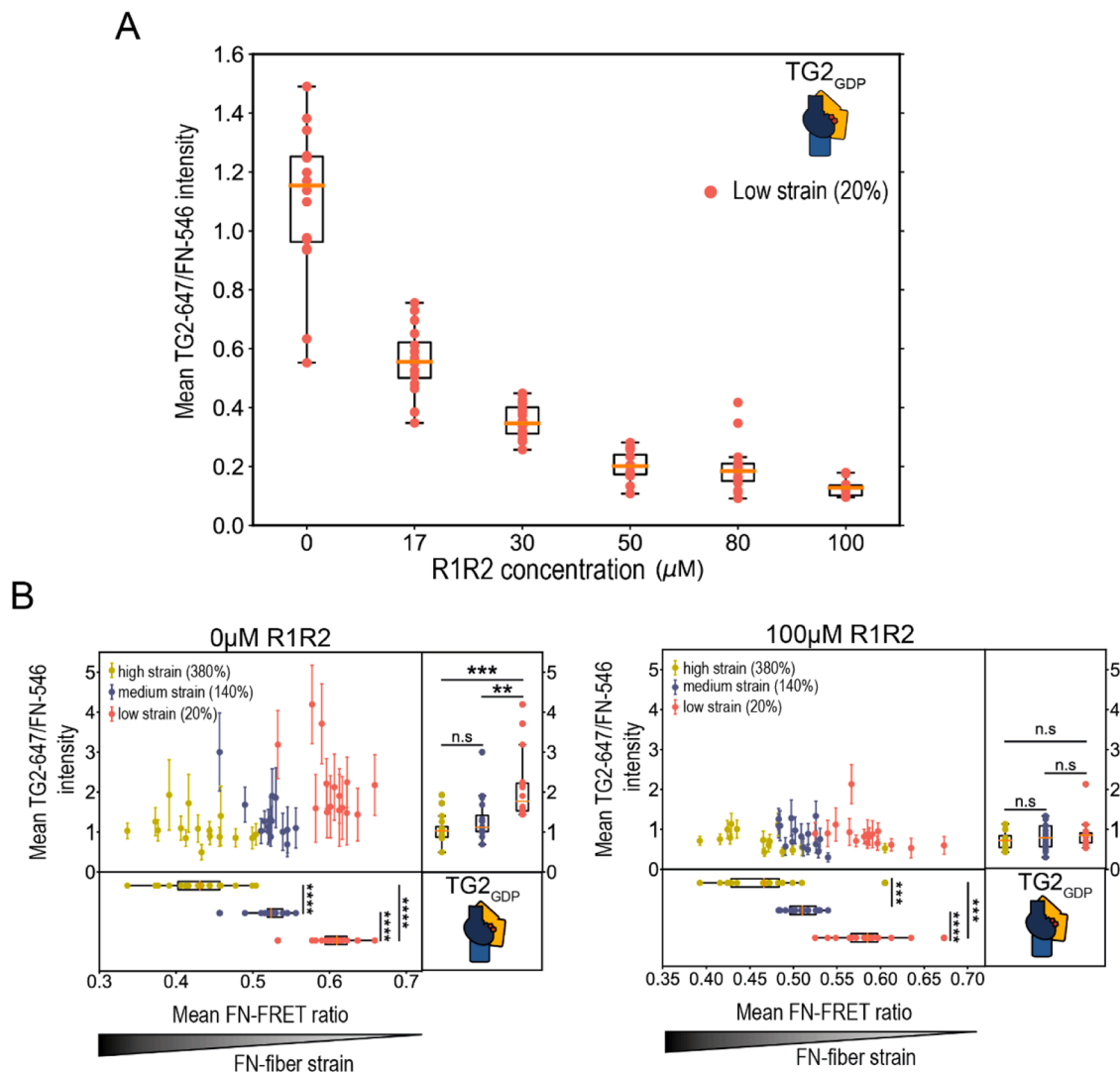


Fig. 7. FN fiber stretch assay reveals a dose-dependent competition between the collagen-mimicking peptide R1R2 and WT gpTG2_{GDP} for binding to FN fibers under high, as well as low strain. A: In the presence of increasingly higher concentrations of R1R2, which targets FN's GBD, TG2_{GDP} binding to the FN fibers under low strain is reduced in a dose-dependent manner. B: Saturating concentrations of R1R2 abolished mechano-regulated TG2 binding to FN, thus limiting TG2 binding to its known canonical binding site. In the presence of 100 μM R1R2, TG2 bound equally to FN fibers under high, medium, and low strain. 15 fibers were analyzed per membrane strain. Statistical significance was computed with Wilcoxon rank-sum statistic for two samples. *p*-values: (* $0.01 \leq p < 0.05$; ** $0.001 \leq p < 0.01$; *** $10^{-5} \leq p < 0.001$; **** $10^{-6} \leq p < 10^{-5}$; ***** $p < 10^{-6}$).

by synergistic interactions of C-terminal TG2 domains with FNI₂₋₃, FNI₈₋₉, or FNIII₁₄₋₁₅ modules, offering multiple options for the high affinity interaction that we observed in our FN fiber stretch assays. FN fiber stretching might thus destroy TG2's multivalent binding motif that is comprised of several FN modules, i.e., by increasing the relative distance between FNI₇, FNI₈ and FNI₉. While TG2's N-terminal residues Lys30, Arg116, His134 bind to FNI₇ with high affinity, we propose here that TG2's C-terminal domains can further enhance this interaction by simultaneously binding to FNI₈ and FNI₉, however, only when FN is in an unstretched conformation (Fig. 8A). Additional interactions of TG2's C-terminal domains with other multidomain fragments of FN, i.e., with FNI₂₋₃, or with FNIII₁₄₋₁₅, might also stabilize FN-TG2 complexes as revealed by XL-MS followed up by structural modelling (Fig. 6). While MS averages over large populations of inter-protein interactions, structural modelling suggests that the C-terminal binding interface of TG2 with FNI₂₋₃ and FNIII₁₄₋₁₅ might partially overlap. Note furthermore, that these binding epitopes are also prone to get disrupted by FN fiber stretching as well, as stretching increases the relative distances of these tandem FN modules too and thus the multivalent binding motif with

TG2.

When discussing TG2 localization outside of the cell, two distinct pools of TG2 are typically noted: TG2 located on the cell surface and TG2 located in the ECM, which appear to perform different functions and interact with different binding partners [19]. On the cell surface, where TG2 acts as an adhesion co-receptor for FN [21], it primarily associates with integrins and the heparan sulfate proteoglycan syndecan-4, forming ternary and/or quaternary adhesive complexes with FN [19,20,93]. Recent advances in understanding of TG2-syndecan-4 interactions suggest that this interaction stabilizes TG2 in a closed conformation, due to a composite binding site consisting of two clusters that form a single high affinity heparin-binding site when brought in proximity in a closed conformation [94,95]. Our data now suggest an additional mechanism that might stabilize this heterocomplex with FN and Syndecan-4, as the synergistic interactions of TG2 N- and C-terminal domains with FN are expected to stabilize TG2's closed conformation despite high (millimolar) extracellular Ca²⁺ concentrations. These quaternary complexes of FN, TG2, Syndecan-4 and β 1-integrins are veritable signaling hubs and can elicit downstream RhoA-ROCK activation and profibrotic signaling

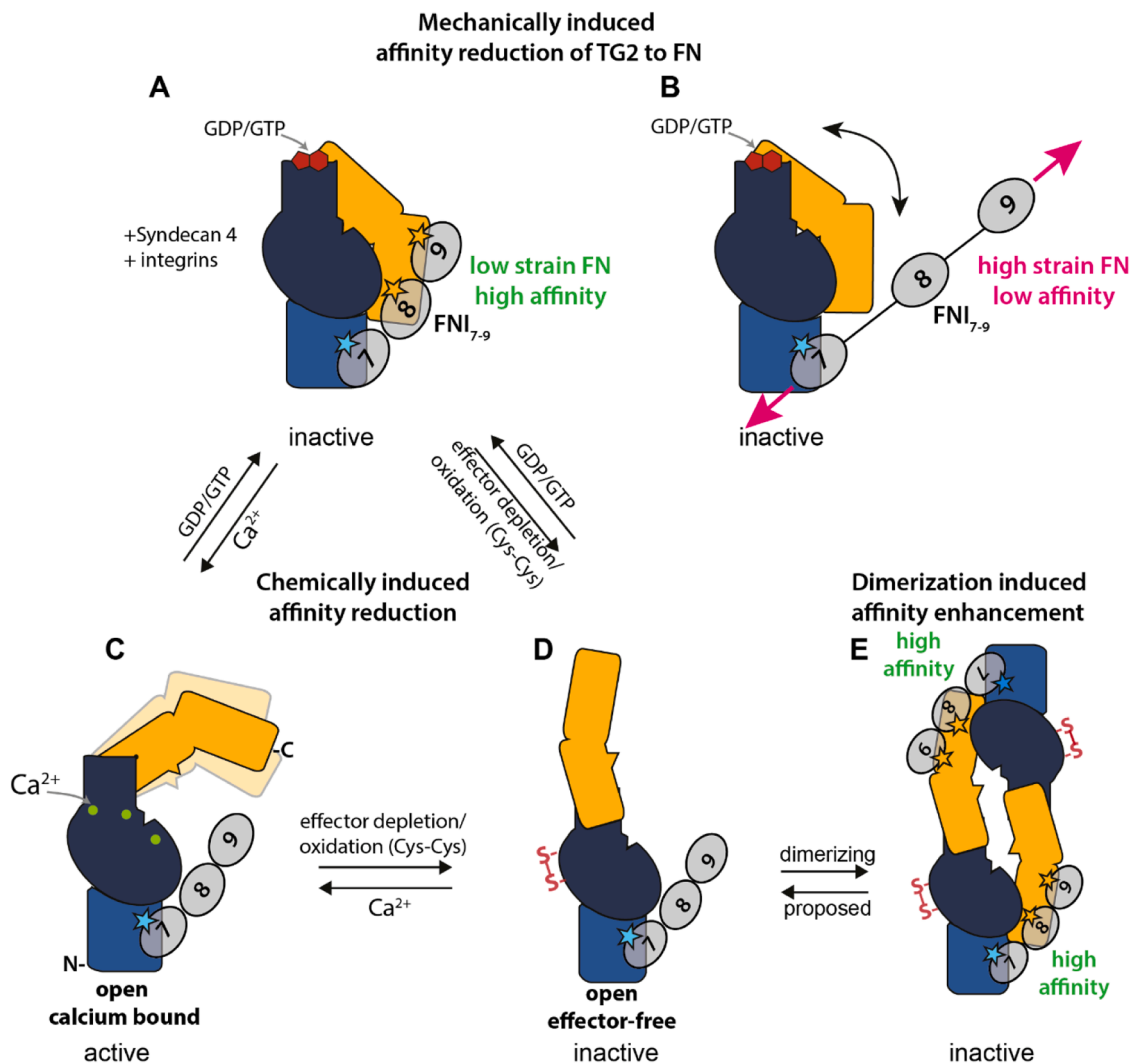


Fig. 8. Sketch illustrating the proposed model of TG2's mechano-regulated binding to FN fibers. A, C, D: TG2 interacts differently with FN fibers depending on the conformational state of TG2 and (B) tensional state of FN fibers. (A): TG2 in its compact and inactive conformation. When TG2's N-terminal β -sandwich is in spatial proximity to its C-terminal β -barrel 2, FNI₇ to the N-terminal domain of TG2 (light blue), while the tandem domains FNI₈₋₉ bind to TG2's C-terminal domains (yellow), enhancing synergistically the interaction. (B) Mechanically induced affinity reduction. When mechanical forces acting on FN fibers stretch the FN modules apart, the multivalent TG2-FN interactions are destroyed and TG2 can bind FN only via its canonical binding site. (C): Chemically induced affinity reduction by calcium binding. Calcium binding causes C-terminal β -barrels to move away from the N-terminal domain, and TG2 assumes distinct open states that are catalytically active. In this case, TG2's C-terminal β -barrels are out of reach and FN can bind only to TG2's N-terminal β -sandwich domain, forming a lower affinity interaction. (D) Chemically induced affinity reduction by formation of a disulfide bond redox-sensitive cysteines (Cys230, Cys370, Cys371). Oxidation of TG2 in the ECM inhibits its catalytic activity. Although oxidized TG2 adopts the open conformation (effector-free), it could still form a high affinity synergy interaction with FN through dimeric TG2 association. (E) Dimerization induced affinity enhancement. Spatial proximity between N-terminal and C-terminal domains could be achieved locally, in which case the domains would be provided by two different TG2 molecules of a TG2 homodimer. Parallel alignment of FNI₇₋₉ modules with TG2's C-terminal β -barrel domains was predicted by crosslink-guided docking.

effects, amongst others [21,93]. Formation of a heterocomplex between FN-TG2 and β 1-integrins, contributes to cell survival and has been implicated in several pathologies. For instance, TG2 enhances ovarian cancer cell anchoring to fibronectin, promoting metastasis [96]. In breast cancer, cooperation between TG2, integrins, and fibronectin enhances cell attachment, invasion and survival [28]. In the ECM of multiple sclerosis lesions, TG2 enhances adhesion and migration of astrocytes on fibronectin in the ECM, which contributes to glial scarring [97,98]. Noteworthy, TG2 also promotes FN fiber deposition in multiple sclerosis lesions [99,100] and in glioblastoma [101].

Can TG2 be stored in the ECM in an inactive conformation even in the presence of oxidative environment? In the ECM, TG2 predominantly co-localizes with the FN matrix, although to a lesser extent, TG2 may also associate with other non-FN interaction partners, such as collagen VI [102]. Unlike on the cell surface, TG2 in the ECM is likely to adopt an

open, effector-free conformation due to oxidation and the formation of a Cys370-Cys371 disulfide bridge [40]. SAXS measurements by Singh *et al.* demonstrated that constitutively open TG2 mutants form homodimers in solution [103]. The fit of TG2 in the extended conformation into the envelope suggests that the two monomers dimerize in an overlapping head-to-tail configuration. Another independent study found that homodimer formation in wild type TG2 is increased at higher temperatures [104]. The authors also used SAXS to measure the multimerization state of TG2 and, like Singh *et al.*, found that the fitting into the SAXS envelope resulted in a head-to-tail homodimer configuration. It can be speculated that a fraction of TG2 in this dimeric state could be immobilized on FN-matrix fibrils in the ECM and be stored there in an inactive state until the requirement for TG2 crosslinking arises to stabilize the matrix in case of injury. As we previously discovered that FN fibers are highly stretched under homeostasis in most healthy organs

[105], this suggests a plausible mechanism for storing inactivated oxidized TG2 dimers bound head-to-tail with lower affinity to stretched than to relaxed FN-matrix fibers. As FN fibers get cleaved at sites of injury, or proteolytically cleaved at sites of inflammation, the structurally relaxed FN will compete effectively for TG2 dimer binding. We thus propose here that this tension dependent switch might allow TG2 storage in ECM of healthy organs, and for fast recruitment of TG2 to damaged FN fibers in case of injury. Supporting this idea, it has been shown that TG2 bound to FN-matrix can be reduced by the enzymatic activity of Thioredoxin and recruited in this way for the crosslinking activity of matrix proteins [71]. Future research should investigate whether a TG2 homodimer can bind fibrillar FN and if such binding can be regulated by FN fiber strain.

Bringing our findings that TG2 binding is modulated by FN fiber tension together with the existing literature, we propose a novel model of mechano-regulated TG2-FN interactions and how this might tune TG2's catalytic activity (Fig. 8). TG2 is inactive when TG2's N-terminal and C-terminal domains are in spatial proximity due to GDP/GTP binding and/or when TG2 interacts with syndecan-4 [94]. We propose here that TG2 and FN can form additional interactions due to the C-terminal β -barrels making synergistic contacts with FN₈₋₉, while TG2's N-terminal domain interacts with FN₁₇ (Fig. 8A) and/or FN₂₋₃ and FN₁₄₋₁₅. Upon FN fiber stretching, the multivalent binding motif is disrupted by, for example, increasing distances between FN₁₇, FN₈ and FN₉ modules, therefore reduced affinity interactions can be formed (Fig. 8B). When TG2 C-terminal domains move away due to calcium binding (Fig. 8C) or oxidation (Fig. 8D), it forms reduced affinity interaction with FN, since C-terminal domains are out of reach. Finally, we propose that oxidized TG2 could form high affinity interactions with adjacent FN fibers due to dimeric TG2 association thus perhaps serving as physical crosslinker as well (Fig. 8E). In this case, spatial proximity between C-terminal and N-terminal domains could be achieved locally within such homodimer. More research is required to establish the physiological role of this homodimer and its binding mode to fibrillar FN.

Therefore, our results indicate that, like for Syndecan-4 [94] or $\alpha 5\beta 1$ integrins, the FN-binding epitope on TG2 is conformational. Interestingly, studies have identified anti-TG2 autoantibodies that induce a shift in a pool of effector-free TG2 either toward the “closed” or “open” conformation, depending on the epitope on TG2 they bind to [41,106]. Although the exact reasons are not known, this could be a common regulatory mechanism shared by many TG2 binding partners to exert an effect on TG2 conformation and thereby, its function.

In organs, FN fiber tension can vary significantly during growth and homeostasis, or upon injury and pathological transformation which are typically accompanied by ECM fiber cleavage [1,3,4,105]. In an in vitro microtissue culture assay, we recently observed that cellular decision-making occurs when FN fiber tension switches from highly stretched in the microtissue growth front that is rich in myofibroblasts, to relaxed fiber tension in the collagen rich maturing core, where fibroblasts are prevalent [107]. A well-tuned tenascin-C, TG2, and matrix metalloprotease driven matrix remodeling activity was crucial to mediate the myofibroblast-fibroblast transition in this in vitro model [107]. It can be speculated that in this transition zone the mechano-regulated TG2 storage and release mechanisms and mechanosensory regulation of cellular behavior are of great significance. We also recently demonstrated that tumor tracks are bordered by an endothelial-like basement membrane and are enriched in their interior with low-tension FN fibers in proximity to a high tenascin-C content [108]. As such, our findings that the interaction of TG2 with FN is tuned by its fiber tension are highly significant.

The cell-ECM interactions are reciprocal and cell forces can tune the exposure of binding sites on ECM proteins [55]. This enables the creation of highly complex ECM environments that consist of a multitude of structural and soluble factors in organ-specific cell niches, representing biophysical and biochemical stimuli acting as simultaneous regulators of

cell behavior. Our observation that the collagen-mimicking peptide R1R2 and TG2 competes for the same binding site on fibrillar FN suggests that the composition of the ECM affects the interaction of its components, which in turn may change cell behavior. This is physiologically relevant because the presence of the R1R2 peptide hampers the myofibroblast-to-fibroblast transition in 2 and 3D cell culture [107, 109]. Proposed shifts in the availability of TG2 in the “closed” or “open” conformation, driven by FN fiber tension, is also likely to modulate TG2 storage and release of TGF β 1 in the ECM [110,111]. Given the role of excessively activated TG2 in fibrosis and cancer [6,31,32], this notion might stimulate a wide variety of new strategies attempting to inhibit tumor stroma and scar fibrosis, which so far include epigenetic modulators, and inhibitors of ECM crosslinking, mechanotransduction and integrin-mediated TGF β activation [112]. Beyond its well described function, our data suggest that TG2 can serve as a FN fiber strain sensor, thereby modulating cell-ECM interactions depending on the tensional state of ECM fibers, including cell adhesion, spreading and migration, as well as cell phenotype modulation. And reciprocally, FN-fibers could serve as a reversible ECM storage space for TG2. These properties of the TG2-FN interactions would thereby modulate tissue responses in homeostasis, tissue growth and repair, as well as under pathological conditions, including fibrotic pathologies and cancer.

Materials and methods

Reagents

Reagents were purchased from Sigma Aldrich, if not mentioned otherwise. Guinea pig liver transglutaminase (gpTG2), Zedira, T006; human tissue transglutaminase (hrTG2, recombinantly produced in *E. coli*), Zedira, T002; short human tissue transglutaminase, aa 1-465 (short hrTG2, barrel 1 and 2 deletion mutant, recombinantly produced in *E. coli*), Zedira (T167); inactive human tissue transglutaminase (Cys277Ser mutant, recombinantly produced in *E. coli*), Zedira (T018); Z-DON-Val-Pro-Leu-OMe, Zedira, (Z006); R1R2 peptide [90,113] (amino acid sequence: GLNGENQKEPEQGERGEAGPPLSGLSGNNGRPSLPLNGENQKEPEQGERGEAGPP) was manufactured by GenScript; Alexa Fluor 647 NHS Ester (A20006), ThermoFisher; Alexa Fluor 488 NHS Ester (A20000), ThermoFisher; Alexa Fluor 546 C5 Maleimide (A10258), ThermoFisher; fibronectin proteolytic fragment from human plasma collagen/gelatin-binding domain (GBD), 45 kDa, F0162, Sigma Aldrich; anti-fibronectin antibody, gelatin binding domain, clone IST-10, from mouse 1 mg/ml (MAB1892), Sigma Aldrich; secondary pAb (ab150107) DK anti-mouse (to MS IgG) (2 mg/ml), Abcam; guanosine 5'-diphosphate disodium salt (GDP), G7127 Sigma Aldrich; silicone sheeting, .010" NRV G/G 40D 12"x12", SMI specialty manufacturing, inc.; Slide-A-Lyser Dialysis Cassette, 20,000MWCO, 66005 ThermoScientific; centrifugal filter units Amicon Ultra – 0.5 ml, 30 K UFC503096 Merck Millipore; disposable PD-10 desalting columns, GE17-0851-01 Merck Millipore; Amicon Ultra 0.5 ml Ultracel 30k Centrifugal filter units, Merck, Millipore; L-Glutathione oxidised (GSSG), G4376-5 G, Lot#SLCJ0220, MW: 612.63 g/mol.

FN isolation from human plasma

Fibronectin (FN) was isolated from human plasma according to a previously described protocol [51]. Briefly, 2 mM phenylmethylsulphonyl fluoride (PMSF) and 10 mM ethylenediaminetetraacetic acid (EDTA) were added to human plasma (Zürcher Blutspendedienst SRK) and centrifuged at 15,000 g for 40 min. Next, plasma was passed through a size-exclusion column (PD-10 Desalting columns, GE Healthcare) and loaded onto a gelatin-sepharose 4B column (VWR Schweiz). After washing with phosphate buffered saline (PBS+10 mM EDTA), NaCl (1 M in PBS) and arginine (0.2 M in PBS), FN was eluted with 1.5 M arginine in PBS. For FRET labelling of FN with donors and acceptors, the gelatin-sepharose 4B column was washed with

1 M NaCl, 1 M urea, and was eluted from the column with 6 M urea. FN purity was checked by SDS-PAGE and western blotting (data not shown). The purified FN was aliquoted and stored in 1.5 M arginine in PBS at -80°C .

Fluorescence labelling of FN and transglutaminases

FN and TG2 were labelled with Alexa fluorophores (AF) on primary amines with AF488-NHS-ester (for FN fiber stretch assay with calcium titration) and AF674-NHS-ester respectively, to obtain FN-488 and TG2-674 according to the manufacturer's instructions (ThermoFisher). Briefly, the buffer was exchanged to carbonate-bicarbonate labelling buffer (0.2 M NaHCO_3 – Na_2CO_3 , pH 8.5) using Slide-A-Lyser dialysis cassettes. Next, FN was incubated with 40-fold molar excess of AF488-NHS-ester, and transglutaminases with 45-fold molar excess of AF647-NHS-ester for 1 h at RT on rotator. Free dye was removed by buffer exchange with 50 mM Tris, pH 7.4, using Slide-A-Lyser dialysis cassettes. The protein purity, concentration and degree of labelling were assessed by spectrophotometric measurements of absorbances at 280 nm, 488 nm, and 647 nm. Proteins were aliquoted, snap frozen in liquid nitrogen and stored at -20°C .

FN labelling with donors and acceptors for FRET

FN was labelled for FRET as previously described [51,69]. Briefly, FN-dimer was doubly labelled on primary amines with AF488 (donor), and with AF546 (acceptor) on the four free cryptic cysteines in modules FNIII₇ and FNIII₁₅. Briefly, FN was denatured in 6 M Urea by addition of equal volume of 8 M guanidine hydrochloride and incubated for 1 h at RT with 20-fold molar excess of AF546-maleimide. Free dye was removed with buffer exchange to carbonate-bicarbonate buffer (0.2 M NaHCO_3 – Na_2CO_3 , pH 8.5) using size-exclusion chromatography (PD-10 Desalting columns, GE Healthcare). Next, FN in carbonate-bicarbonate buffer was immediately incubated on rotator with a 40-fold molar excess of AF488-NHS-ester for 1 h at room temperature. Afterwards, free dye was removed by buffer exchange to PBS, pH 7.4 using PD-10 Desalting columns. The protein purity, concentration and degree of labelling were assessed by spectrophotometric measurements of absorbances at 280 nm, 488 nm, and 546 nm. FN-FRET was aliquoted, snap-frozen in liquid nitrogen and stored at -80°C . To construct FN-FRET denaturation curve in order to assess the correlation of the FRET signal to the loss of FN tertiary and quaternary structure in solution, FN-FRET was chemically denatured with increasing concentrations of guanidine hydrochloride as was previously described [51, 69]. Briefly, the coverslips were blocked with 4% bovine serum albumin (BSA) for 1 h at RT, then washed with PBS. FN-FRET was mixed with an equal volume of guanidine hydrochloride in PBS to a final concentration of 0 M, 0.5 M, 1 M, 2 M, 3 M, and 4 M and incubated for 1 h at RT. To separate FN dimer to monomers, disulfide bonds between two FN monomers were reduced with 50 mM DTT for 1 h at RT, before incubating FN-FRET with 1 M guanidine hydrochloride. A droplet from each solution was added onto the prepared coverslip and imaged using Olympus FV1000 confocal microscope as described below.

FN fiber stretch assay

FN fiber stretch assay was performed as was previously described [59,63]. FN fibers were manually pulled from a droplet of 0.4 mg/ml FN solution (to avoid inter-molecular FRET, not more than 10% FN-FRET probes were added) with the needle tip and deposited on the silicone sheet mounted on the custom-made uniaxial stretch device. For the single fiber studies, 15 fibers were deposited parallel to the stretch axis. To create intersecting fibers, 10 fibers were deposited both parallel and perpendicular to the stretch axis (Fig. 2A). Next, FN fibers were washed with PBS, and silicone sheets were stretched, relaxed, or left unchanged (native), subjecting the silicone membranes to strains of 100%, -50% or

0% respectively. Previous calibration studies converted the silicone membrane strains to the respective FN fiber strains of 380% (stretched membrane: high FN fiber strain), 20% (relaxed membrane: low FN fiber strain) and 140% (native membrane: medium FN fiber strain) parallel to the stretch axis and 90% (stretched membrane), 219% (relaxed membrane) and 140% (native membrane) perpendicular to the stretch axis [67]. Though the native membrane is not subjected to any strain, FN fibers are typically pre-strained to $\sim 140\%$ due to the forces required to pull them out of the droplet [67]. Next, FN fibers were blocked with 4% BSA for 30 min at RT, then washed with PBS. Transglutaminases were induced into a specific conformation by 30 min pre-incubation with corresponding allosteric effectors, immediately added to FN fibers at a concentration of 10 $\mu\text{g}/\text{ml}$ TG2–647 in 50 mM Tris, and incubated for 1 h at RT. TG2 solutions were added to FN fibers and incubated on fibers for 1 h at RT. This was followed by 3 times washes for 5 min each with 50 mM Tris and fixation with 4% PFA in PBS for 15 min at RT. FN fibers were imaged immediately using Olympus FV1000 confocal microscope. For FN fiber stretch assays recombinantly produced in *E.coli* TG2 and guinea pig liver TG2 were used. The data shown in Fig. 2, Fig. 3 A-C were obtained with recombinantly produced TG2.

Induction of conformational changes of TG2 with its allosteric effectors

To induce the closed conformation (TG_{GDP}), 10 $\mu\text{g}/\text{ml}$ TG2–647 was pre-incubated for 30 min at RT in 1 mM GDP, 1 mM EDTA in 50 mM Tris. To induce catalytically active open conformation, TG2 was pre-incubated for 20 min at RT in 1.2 mM CaCl_2 in 50 mM Tris. To induce catalytically inactive extended conformation (effector-free on Fig. 2A), TG2 was pre-incubated with 100 μM “Z-DON” Z006 (Zedira) in 5 mM CaCl_2 in 50 mM Tris for 30 min at RT. To get rid of free Z006, the solution was passed through centrifugal filter units (Ultracel 30k, Merk, Millipore), according to manufacturer's instructions, and TG2 bound to Z006 “Z-DON” (TG2_{Z006}) was resuspended in 50 mM Tris or 1.2 mM CaCl_2 in 50 mM Tris. To oxidise TG2 (oxTG2), guinea pig liver TG2 (gpTG2) was incubated in 2 mM GSSG and 1 mM EDTA in 50 mM Tris for 3 h at 37°C . oxTG2 was passed through centrifugal filter units and resuspended in 50 mM Tris.

A dose-response competition experiment of TG2 with the R1R2 peptide

A dose-response competition study with R1R2 peptide and a constant concentration of TG2_{GDP} (10 $\mu\text{g}/\text{ml}$ guinea pig liver TG2) was performed using only horizontally pulled FN-FRET fibers (parallel to the stretch axis) on relaxed membranes (low FN fiber strain). After blocking FN fibers with BSA, 10 $\mu\text{g}/\text{ml}$ TG2_{GDP} labelled with AF647 was added to the fibers together with R1R2 peptide at one of the concentrations: 0 μM , 17 μM , 30 μM , 50 μM , 80 μM and 100 μM . TG2_{GDP} and R1R2 were diluted in 1 mM GDP, 1 mM EDTA, 1 mM MgCl_2 in 50 mM Tris. Solutions were incubated on FN fibers for 1 h at RT, FN fibers were washed 3 times for 5 min with 50 mM Tris and fixed with 4% PFA in PBS for 15 min at RT.

Calcium dose-response experiment

For calcium dose-response experiments, FN labelled only with AF488 was used and guinea pig liver TG2 (gpTG2) was labelled with AF-647. Like R1R2 competition studies, only horizontally pulled FN-AF488 fibers (parallel to the stretch axis) on relaxed membranes (low FN fiber strain) were used for this experiment. 10 $\mu\text{g}/\text{ml}$ gpTG2 was pre-incubated for 20 min at RT with 1 μM , 100 μM , 250 μM , 500 μM , 1.2 mM, 5 mM, and 10 mM CaCl_2 in 50 mM Tris. 10 $\mu\text{g}/\text{ml}$ gpTG2 pre-incubated in 1 mM GDP, 1 mM EDTA in 50 mM Tris and 10 $\mu\text{g}/\text{ml}$ gpTG2 pre-incubated in 1 mM EDTA in 50 mM Tris were used as controls. gpTG2 solutions were incubated on the fibers for 1 h at room temperature, followed by 3 times for 5 min washes and fixation with 4% PFA in PBS. z-stacks of 3 focal planes with steps of 1micron were obtained with Nikon VisiTron Spinning disk confocal, 60x water immersion objective,

using 488 and 640 lasers and confGFP and confCy5 emission filter cubes. Images were analyzed with custom-written Python script. Briefly, Gaussian filter (sigma=1) was applied to both FN and TG2 channels, FN channel was thresholded using Otsu algorithm and binary mask created, the mask was applied to both the FN and TG2 channel, replacing all background pixels with NaN, which were excluded from analysis. Then, TG2 signal was normalized pixel-by-pixel to the FN signal (TG2-647/FN-488), and the mean normalized TG2 intensity was calculated over the maximum intensity projection of the normalized TG2 signal.

FRET confocal microscopy of FN fibers with bound TG2-647

Z-stacks parameters were set so that the acquisition of stacks of three images always started from the top surface of an FN fiber, moving inside the fiber interior (toward silicone membrane), first by 1 and then by 2 μm . Z-stack images were acquired with Olympus FV1000 confocal microscope with 0.9NA 40X water immersion objective, according to a procedure described in detail previously [63]. Briefly, image acquisition was performed in three sequential steps with five channels using excitation and detection windows as depicted in Supplementary Fig. 1. Donor, acceptor, and FRET intensities were measured with 12 nm bandwidths over acceptor and donor emission peaks. TG2-647 excitation and detection were always performed in a separate channel (channel 5), to avoid unwanted crosstalk from the donor AF488 and acceptor AF546 signals upon excitation with 488 nm and 543 nm lasers. FRET-signal correction due to the bleed-through of both donor and acceptor signals into the FRET-excited acceptor channel was performed as was described in detail previously [63,114], and an example of the calculation of β - and γ -correction factors is shown in Supplementary Fig. 1. Acquisition parameters (laser intensity and PMT voltage) were set to maximize the detected signal, while minimizing bleaching and background signal, and were kept constant throughout the experiment.

Ratiometric FRET image analysis and a correlation of TG2-647 binding with FN-FRET ratio

Ratiometric FRET signal calculation and a correlation of TG2-647 signal to the FN-FRET ratios was performed pixel-by-pixel using custom written Matlab script, which was validated and described in detail before [63]. Briefly, images from different channels were aligned using “imregister” Matlab function, thresholded, mean background signal subtracted, and a mask generated. To remove the pixels at the edges of fibers, where light scattering can create false FRET values, edges of the mask were eroded, then a local 3×3 averaging filter and a one-deviation Gaussian averaging filter were applied. FRET ratios were calculated by dividing pixel-by-pixel the corrected intensity from the acceptor emission due to FRET (channel 1 in Supplementary Fig. 1) by the donor emission (channel 2 in Supplementary Fig. 1). Since the intensity of TG2 signal is dependent on the amount of FN to which it binds, we normalized the TG2-647 signal (channel 5 in Supplementary Fig. 1) by dividing it pixel-by-pixel by the directly excited acceptor AF546 (channel 3 in Supplementary Fig. 1): TG2-647/FN-546. Examples of raw confocal images and corresponding color-coded pixel-by-pixel result after the image processing are shown in Supplementary Fig. 3 (intersecting fibers) and Supplementary Fig. 5 (horizontal fibers). To plot the mean, maximum intensity projections (MIP) of obtained three-dimensional arrays were taken and the mean intensity of FN-FRET ratio and mean intensity of TG2-647 signal were calculated from MIP and plotted as mean scatterplots. To relate each pixel FN-FRET value with its corresponding TG2 pixel intensity, they were plotted versus each other as two-dimensional density plots (Supplementary Fig. 4).

Statistical analysis for FN fiber stretch assay data

Since not all data had a normal distribution, statistical significance between groups was assessed by the nonparametric two-sided Wilcoxon

rank sum statistic for two samples, which does not imply data distribution normality, as was performed previously in a similar study [63]. Statistical significance was assessed for $*0.01 \leq p < 0.05$; $**0.001 \leq p < 0.01$; $***10^{-5} \leq p < 0.001$; $****10^{-6} \leq p < 10^{-5}$; $*****p < 10^{-6}$.

Microplate FN-TG2 binding assay

To determine the concentrations of full-length FN and with 45kDa-FN at which microtiter plates would be coated with approximately similar number of binding sites for TG2, titration experiments were carried out. For this, 96-well black flat non-transparent bottom microtiter plates were coated with 0.1, 0.2, 0.4, 0.6, 0.8, 1, 2, 5, 10, 20, 30 and 50 $\mu\text{g}/\text{ml}$ full-length FN or 45 kDa-FN GBD in PBS at 4°C overnight. Wells were washed with PBS 3 times for 5 min and blocked for 30 min with 4% BSA in PBS, followed by another wash. Full-length FN and 45 kDa-FN GBD were detected with monoclonal mouse anti-FN antibody with epitope within GBD (MAB1892, Sigma), clone IST-10 (1:1000 in 2% BSA in PBS) for 1 h at RT, followed by incubation with anti-mouse pAb ab150107 AF647 (1:1000 in 2% BSA in PBS) for another 1 h at RT, and finally fixation with 4% PFA for 10 min. After each antibody incubation wells were washed with PBS 3 times for 5 min. Fluorescence intensity was measured with Tecan Spark plate reader. Obtained data were fit using a four-parameter logistic (4PL) curve. Next, the concentration of the full-length FN at which 95% of maximum intensity was reached were calculated from the curve as 2.4 $\mu\text{g}/\text{ml}$. Then, the concentration of 45 kDa-FN GBD, which corresponded to the 95% of full-length FN intensity was calculated from the curve as 0.6 $\mu\text{g}/\text{ml}$. In all subsequent experiments, microtiter plates were coated with 2.4 $\mu\text{g}/\text{ml}$ of full-length FN and 0.6 $\mu\text{g}/\text{ml}$ of 45 kDa-FN GBD.

For experiments with wild type gpTG2 and short hrTG2, 96-well black flat non-transparent bottom microtiter plates were coated with either 2.4 $\mu\text{g}/\text{ml}$ full-length FN or 0.6 $\mu\text{g}/\text{ml}$ 45 kDa-FN at 4°C overnight. After incubation, wells were washed 3 times for 5 min with 50 mM Tris and blocked for 30 min with 4% BSA in 50 mM Tris at RT. TG2-647 solutions of 0.1, 0.5, 1, 2, 3, 5, 7, 10 $\mu\text{g}/\text{ml}$ were prepared in either 1 mM GDP, 1 mM EDTA in 50 mM Tris, or 1 mM EDTA in 50 mM Tris, or 1.2 mM CaCl_2 in 50 mM Tris, or 1.2 mM CaCl_2 , 100 μM Z006 in 50 mM Tris and pre-incubated for 20 min at RT. Transglutaminase dilutions were added to the FN-coated wells and incubated at RT for 1 h. Wells were washed 3 times for 5 min with 50 mM Tris and fixed with 4% PFA for 10 min. Fluorescence intensity was measured with Tecan Spark plate reader. Obtained data were fit using a four-parameter logistic (4PL) curve and plotted.

Chemical crosslinking

TG2 (human recombinant) was incubated either with full-length FN, or the 45-kDa FN fragment in 1 mM GDP, 1 mM EDTA in PBS for 1 hr at room temperature. Crosslinking experiments were performed with 50 μg total protein at concentrations of approximately 0.7 mg/ml for samples containing full-length fibronectin and at approximately 0.25 mg/ml for samples containing the 45-kDa FN (GBD). All steps were performed on a ThermoMixer (Eppendorf) at 750 rpm.

Lysine crosslinking with a 1:1 mixture of non-deuterated and deuterated disuccinimidyl suberate (DSS- d_0/d_{12} , Creative Molecules) was initiated by adding the crosslinking reagent from a freshly prepared 25 mM stock solution in dimethyl formamide to a final concentration of 1 mM [115]. The reaction was allowed to proceed for 60 min at room temperature (23°C) before adding ammonium bicarbonate to a final concentration of 50 mM and incubating further for 30 min.

Crosslinking of carboxyl groups and of amine groups with carboxyl groups was performed using non-deuterated and deuterated pimelic dihydrazide (PDH- d_0 , ABCR, and PDH- d_{10} , Sigma-Aldrich) and the coupling reagent 4-(4,6-dimethoxy-1,3,5-triazin-2-yl)-4-methylmorpholinium (DMTMM) chloride (Sigma-Aldrich). Stock solutions were prepared in phosphate-buffered saline at concentrations of 140

mM (PDH, 1:1 mixture of d₀ and d₁₀) and 520 mM (DMTMM). Two different reaction conditions were used for combined PDH/DMTMM crosslinking: 44 mM PDH and 88 mM DMTMM or 22 mM PDH and 11 mM DMTMM, respectively [116]. Samples were incubated for 60 min at room temperature and the reaction was stopped by passing the sample solutions through a Zeba spin desalting column (ThermoFisher Scientific) according to the manufacturer's instructions. Quenched samples solutions were subsequently evaporated to dryness in a vacuum centrifuge.

Sample processing and mass spectrometric (MS) analysis

Dried samples were dissolved in 50 µL of 8 M urea solution. Cysteine thiols were reduced by addition of tris(2-carboxyethyl)phosphine to a final concentration of 2.5 mM and incubation for 30 min at 37°C, and free thiol groups were alkylated with iodoacetamide (final concentration of 5 mM, incubation for 30 min at room temperature, protected from light) prior to enzymatic digestion.

Proteolysis with endoproteinase Lys-C and trypsin was performed as follows: The reduced and alkylated samples were diluted to 5.5 M urea with 150 mM ammonium bicarbonate solution and Lys-C (Wako) was added at an enzyme-to-substrate ratio of 1:100. After incubation at 37°C for 2 h, the solutions were further diluted to 1 M urea with 50 mM ammonium bicarbonate, and trypsin (Promega) was added at an enzyme-to-substrate ratio of 1:50. Trypsin digestion was then allowed to proceed overnight.

Proteolysis with chymotrypsin (Roche) was performed by diluting the solutions to 1 M urea with 50 mM ammonium bicarbonate and adding the protease at an enzyme-to-substrate ratio of 1:50. Samples were incubated for 2 h at 25°C.

Enzymatic digestion reactions were stopped by adding 100% formic acid to a final concentration of 2% (v/v) and samples were purified by solid-phase extraction using 50 mg SepPak tC18 cartridges (Waters). Purified samples were fractionated by peptide size exclusion chromatography (SEC) on an Äkta micro FPLC system equipped with a Superdex 30 Increase column (300 × 3.2 mm, GE/Cytiva). The separation was carried out with a mobile phase consisting of water/acetonitrile/trifluoroacetic acid (30/70/0.1, v/v/v) at a flow rate of 50 µL/min. For each sample, three or four 100 µL fractions from the high mass region were individually collected and evaporated to dryness.

Liquid chromatography-tandem mass spectrometry was performed on an Easy nLC-1200 HPLC system coupled to an Orbitrap Fusion Lumos mass spectrometer equipped with a Nanoflex electrospray ionization source (all ThermoFisher Scientific). Approximately one µg or less for each SEC fraction was injected and the peptides were separated on an Acclaim PepMap RSLC column (150 mm × 75 µm, 2 µm particle size, ThermoFisher Scientific) at a flow rate of 300 nl/min. The mobile phase gradient was set to 11% B to 40% B in 60 min, with mobile phase A = water/acetonitrile/formic acid (98/2/0.15, v/v/v) and B = acetonitrile/water/formic acid (80/20/0.15, v/v/v). The mass spectrometer was operated in the data-dependent, “top speed” acquisition mode with a cycle time of 3 s. Precursor ion spectra were acquired in the orbitrap analyzer at a resolution setting of 120,000. Precursors with a charge state between +3 and +7 were selected for collision-induced fragmentation in the linear ion trap with a normalized collision energy of 35%. For most experiments, fragment ions were detected in the orbitrap analyzer at a resolution setting of 30,000. For some samples, one of the two replicate injections was performed with MS/MS detection in the linear ion trap to achieve higher sensitivity. In that case, fragmentation conditions remained unchanged, and the linear ion trap was operated with a “rapid” scan rate.

Identification of crosslinked peptides

Preliminary experiments found unequivocal evidence for UniProt proteoforms P02751-1 and -9, with isoform 1 having the most

proteotypic peptides. This isoform was therefore included in the sequence database and all numbering refers to it. In addition, the database consisted of the sequence of transglutaminase and the sequence of three contaminants identified from *E. coli*: CH60, SLYD, and ARNA. Target/decoy searches were performed using a decoy database containing the reversed sequences of all database entries.

MS/MS spectra were searched against these databases using xQuest, version 2.1.5 (available from https://gitlab.ethz.ch/leitner_lab) [117]. The crosslinking specificities were set as follows: For DSS, K and the protein N terminus; for PDH, D and E; for DMTMM, K with D and K with E. For Lys-C/trypsin digestion, protease specificity was set to cleavage after K and R unless followed by P, with a maximum of two missed cleavages per peptide allowed (excluding the crosslinking site, if applicable). For chymotrypsin, cleavage was considered after F, L, M, W, and Y, with a maximum number of missed cleavages set to four. Carbamidomethylation of C was treated as a fixed modification, and oxidation of M as a variable modification during the search. The mass error was set to ±15 ppm for orbitrap detection and to 0.2 Da and 0.3 Da for the detection of “common” and “xlink” fragment ion types for detection in the linear ion trap, respectively. All identifications were further filtered for a %TIC value ≥0.1 and a main xQuest score of ≥20 for fragment ion detection in the ion trap and ≥25 for fragment ion detection in the orbitrap analyzer, respectively. MS/MS spectra of the remaining candidates were evaluated and rejected if they did not contain at least four bond cleavages in total per peptide or at least three consecutive bond cleavages per peptide. All crosslink identifications are provided as tables in the Supplementary materials.

Integrative structural modeling and docking

A detailed description of the entire modeling process, which allows for replication of the results is provided in Supplementary Notes 1–3, overview of the modeling workflow is provided in Supplementary Fig. 13. Briefly, I-TASSER [80] was used for structural refinement of available PDB templates of TG2, and FN fragments using experimental crosslinks within those regions as distance restraints (Supplementary Note 1). ROSETTA [83] and AlphaFold [84] were used for modeling of FNI₇₋₉ and 45-kDa FN (GBD), followed by evaluation of resulting structures using QMEAN [85]. Intra-protein crosslinks were used both as distance restraints for structural refinement and for evaluation of resulting models based on their compatibility/non-compatibility with the imposed distance cutoff. To assign compatibility/non-compatibility criteria, Euclidean distances between β-carbons (CB-CB) of the cross-linked residues were calculated using Xwalk [81]. Euclidean distance cut-offs we set as follows: for DSS < 35 Å, ED for DMTMM < 25 Å, ED for PDH < 35 Å, and crosslinks above the set cut-off value were considered as incompatible. Inter-protein crosslinks were validated and active residues predicted using DisVis [87] (Supplementary Note 2). To predict active residues involved in the interaction, we submitted to DisVis server residues with relative solvent accessibility of at least 40% for either the main chain or the side chain. The relative solvent accessibility was calculated using NACCESS [88]. Inter-protein crosslinks that were predicted by DisVis to be incompatible were excluded from further docking steps. Docking was performed with HADDOCK [86]. Detailed description of each docking run, and all used distance restraints are provided in Supplementary Note 3. Experimental inter-protein crosslinks were mapped onto predicted models and Euclidean distances calculated using Xwalk. Obtained structures were visualized with ChimeraX [118].

Data availability statement

The mass spectrometry proteomics data have been deposited to the ProteomeXchange Consortium [64] via the PRIDE [119] partner repository with the dataset identifier PXD043976. Integrative modelling structures have been deposited to PDB-Dev [65] with accession codes PDBDEV_00000216, PDBDEV_00000218, PDBDEV_00000219 and

PDBDEV_0000220.

Significance and conclusions

We discovered here that the binding of a crosslinking enzyme to ECM fibers is mechano-regulated. Mechanical forces acting on ECM fibers can regulate the interactions of TG2 with FN and we suggest a novel mechanism of this mechano-regulated TG2-FN interactions based on combining FN fiber stretch assay with XL-MS studies to decipher a structural mechanism. A previously unknown role of the C-terminal β -barrel domains of TG2 is proposed, i.e. that they serve as a synergy binding site for FN, and are essential for tuning the mechano-regulated binding. In contrast to what was previously assumed, we show that TG2's conformational states affect TG2 interactions with FN, since mechano-regulated binding is only possible when the N-terminal and C-terminal domains of TG2 are in spatial proximity. Thus, our study improves the understanding of the TG2-FN binding interface. This knowledge will also help in future designs of interfering compounds targeting TG2-FN interactions. We thus propose a new role for TG2 as a FN fiber strain sensor and a modulator of cell-ECM interactions in response to the tensional state of ECM fibers. Our model also offers a new perspective into how mechanical forces acting on ECM fibers can reciprocally regulate critical cellular processes of adhesion, spreading, and migration through the mechano-regulation of crosslinking enzymes binding with the ECM.

CRedit authorship contribution statement

Kateryna Selcuk: Conceptualization, Methodology, Software, Validation, Formal analysis, Investigation, Data curation, Writing – original draft, Visualization, Project administration. **Alexander Leitner:** Methodology, Formal analysis, Investigation, Resources, Data curation, Supervision, Writing – review & editing. **Lukas Braun:** Conceptualization, Software, Formal analysis, Writing – original draft. **Fanny Le Blanc:** Formal analysis, Investigation. **Paulina Pacak:** Software, Resources. **Simon Pot:** Writing – review & editing, Funding acquisition. **Viola Vogel:** Conceptualization, Resources, Supervision, Writing – review & editing, Funding acquisition.

Declaration of Competing Interest

None.

Acknowledgements

The authors thank Chantel Spencer for isolating plasma fibronectin, Dr. Mario Benn for discussions and general support, Dr. Zhe Lin for involvement in early experiment with single-labeled FN fibers, Dr. Szymon Stoma (ScopeM) for checking the Python script which outputs normalized pixel-by-pixel FN-488/TG2-647 mean intensity values, Scientific Center for Optical and Electron Microscopy (ScopeM) of ETH Zurich, Joachim Hehl and Dr. Tobias Schwartz from ScopeM for support with Nikon Spinning Disk imaging. AL acknowledges Prof. Dr. Paola Picotti for access to instrumentation and laboratory infrastructure. The authors are grateful to Prof. Dr. Ludvig Sollid and Dr. Jorunn Stammaes at the University of Oslo for discussions on their previous TG2-FN studies. The authors are grateful to Prof. Dr. Elisabetta Verderio Edwards for useful discussions regarding the physiological implications of our findings and the feedback on the manuscript.

FLB was supported by the Swiss-European Mobility Program (SEMP). This study was funded in part by the Velux Stiftung Foundation Project Nr. 1227 (SP), the Swiss National Science Foundation Grant Nr. 175839 (V.V.), as well as the ETH Zurich (VV).

References

- [1] J.D. Humphrey, E.R. Dufresne, M.A. Schwartz, Mechanotransduction and extracellular matrix homeostasis, *Nat. Rev. Mol. Cell Biol.* 15 (2014) 802–812.
- [2] P.A. Janmey, D.A. Fletcher, C.A. Reinhart-King, Stiffness sensing by cells, *Physiol. Rev.* 100 (2020) 695–724.
- [3] O. Chaudhuri, J. Cooper-White, P.A. Janmey, D.J. Mooney, V.B. Shenoy, Effects of extracellular matrix viscoelasticity on cellular behaviour, *Nature* 584 (2020) 535–546.
- [4] M. Valet, E.D. Siggia, A.H. Brivanlou, Mechanical regulation of early vertebrate embryogenesis, *Nat. Rev. Mol. Cell Biol.* 23 (2022) 169–184.
- [5] T. Panciera, A. Citron, D. Di Blasio, G. Battilana, A. Gandin, S. Giullitti, M. Forcato, S. Bicciato, V. Panzetta, S. Fusco, L. Azzolin, A. Totaro, A.P. Dei Tos, M. Fassan, V. Vindigni, F. Bassetto, A. Rosato, G. Brusatin, M. Cordenonsi, S. Piccolo, Reprogramming normal cells into tumour precursors requires ECM stiffness and oncogene-mediated changes of cell mechanical properties, *Nat. Mater.* 19 (2020) 797–806.
- [6] Mario C. Benn, Willi Weber, Enrico Klotzsch, Tissue transglutaminase in fibrosis — more than an extracellular matrix cross-linker, *Curr. Opin. Biomed. Eng.* 10 (2019) 156–164.
- [7] R.L. Eckert, Transglutaminase 2 takes center stage as a cancer cell survival factor and therapy target, *Mol. Carcinog.* 58 (2019) 837–853.
- [8] R.L. Eckert, M.L. Fisher, D. Grun, G. Adhikary, W. Xu, C. Kerr, Transglutaminase is a tumor cell and cancer stem cell survival factor, *Mol. Carcinog.* 54 (2015) 947–958.
- [9] M.V. Nurminkaya, A.M. Belkin, Cellular functions of tissue transglutaminase, in: *International Review of Cell and Molecular Biology* 294, 2012, pp. 1–97. Elsevier Inc.
- [10] D. Telci, M. Griffin, Tissue transglutaminase (TG2) - a wound response enzyme, *Front. Biosci.* 11 (2006) 867–882.
- [11] E.A.M. Verderio, T. Johnson, M. Griffin, Tissue transglutaminase in normal and abnormal wound healing: review article, *Amino Acids* 26 (2004) 387–404.
- [12] H.F. Upchurch, E. Conway, M.K. Patterson, M.D. Maxwell, Localization of cellular transglutaminase on the extracellular matrix after wounding: characteristics of the matrix bound enzyme, *J. Cell. Physiol.* 149 (1991) 375–382.
- [13] N. Agnihotri, K. Mehta, Transglutaminase-2: evolution from pedestrian protein to a promising therapeutic target, *Amino Acids* 49 (2017) 425–439.
- [14] E.A.M. Verderio, D. Telci, A. Okoye, G. Melino, M. Griffin, A novel RGD-independent cell adhesion pathway mediated by fibronectin-bound tissue transglutaminase rescues cells from Anoikis, *J. Biol. Chem.* 278 (2003) 42604–42614.
- [15] R.L. Eckert, M.T. Kaartinen, M. Nurminkaya, A.M. Belkin, G. Colak, G.V. W. Johnson, K. Mehta, Transglutaminase regulation of cell function, *Physiol. Rev.* 94 (2014) 383–417.
- [16] M. Siegel, P. Strnad, R.E. Watts, K. Choi, B. Jabri, M.B. Omary, C. Khosla, Extracellular transglutaminase 2 is catalytically inactive, but is transiently activated upon tissue injury, *PLoS One* 3 (2008) 1–11.
- [17] N.M. Plugis, B.A. Palanski, C.H. Weng, M. Albertelli, C. Khosla, Thioredoxin-1 selectively activates transglutaminase 2 in the extracellular matrix of the small intestine: Implications for celiac disease, *J. Biol. Chem.* 292 (2017) 2000–2008.
- [18] S. Gundemir, G. Colak, J. Tucholski, G.V.W. Johnson, Transglutaminase 2: a molecular Swiss army knife, *Biochim. Biophys. Acta - Mol. Cell Res.* 1823 (2012) 406–419.
- [19] A.M. Belkin, Extracellular TG2: emerging functions and regulation, *FEBS J.* 278 (2011) 4704–4716.
- [20] D. Telci, Z. Wang, X. Li, E.A.M. Verderio, M.J. Humphries, M. Baccarini, H. Basaga, M. Griffin, Fibronectin-tissue transglutaminase matrix rescues RGD-impaired cell adhesion through syndecan-4 and β 1 integrin co-signaling, *J. Biol. Chem.* 283 (2008) 20937–20947.
- [21] S.S. Akimov, D. Krylov, L.F. Fleischman, A.M. Belkin, Tissue transglutaminase is an integrin-binding adhesion coreceptor for fibronectin, *J. Cell Biol.* 148 (2000) 825–838.
- [22] Z. Wang, R.J. Collighan, S.R. Gross, E.H.J. Danen, G. Orend, D. Telci, M. Griffin, RGD-independent cell adhesion via a tissue transglutaminase-fibronectin matrix promotes fibronectin fibril deposition and requires syndecan-4/2 and α 5 β 1 integrin co-signaling, *J. Biol. Chem.* 285 (2010) 40212–40229.
- [23] Z. Wang, D. Telci, M. Griffin, Importance of syndecan-4 and syndecan -2 in osteoblast cell adhesion and survival mediated by a tissue transglutaminase-fibronectin complex, *Exp. Cell Res.* 317 (2011) 367–381.
- [24] S.S. Akimov, A.M. Belkin, Cell-surface transglutaminase promotes fibronectin assembly via interaction with the gelatin-binding domain of fibronectin: a role in TGF β -dependent matrix deposition, *J. Cell Sci.* 114 (2001) 2989–3000.
- [25] L. Yang, S. Friedland, N. Corson, L. Xu, GPR56 inhibits melanoma growth by internalizing and degrading its ligand TG2, *Cancer Res.* 74 (2014) 1022–1031.
- [26] B. Yakubov, B. Chelladurai, J. Schmitt, R. Emerson, J.J. Turchi, D. Matei, Extracellular tissue transglutaminase activates noncanonical NF- κ B signaling and promotes metastasis in ovarian cancer, *Neoplasia* 15 (2013) 609–619.
- [27] M.L. Fisher, J.W. Keillor, W. Xu, R.L. Eckert, C. Kerr, Transglutaminase is required for epidermal squamous cell carcinoma stem cell survival, *Mol. Cancer Res.* 13 (2015) 1083–1094.
- [28] L.S. Mangala, J.Y. Fok, I.R. Zorrilla-Calancha, A. Verma, K. Mehta, Tissue transglutaminase expression promotes cell attachment, invasion and survival in breast cancer cells, *Oncogene* 26 (2007) 2459–2470.
- [29] S.H. Chen, C.Y. Lin, L.T. Lee, G.D. Chang, P.P. Lee, C.C. Hung, W. Te Kao, P. H. Tsai, A.V. Schally, J.J. Hwang, M.T. Lee, Up-regulation of fibronectin and tissue transglutaminase promotes cell invasion involving increased association with

- integrin and MMP expression in A431 cells, *Anticancer Res.* 30 (2010) 4177–4186.
- [30] Y. Bagatur, A.Z. Ilter Akulke, A. Bihorac, M. Erdem, D. Telci, Tissue transglutaminase expression is necessary for adhesion, metastatic potential and cancer stemness of renal cell carcinoma, *Cell Adhes. Migr.* 12 (2018) 138–151.
- [31] L.E. Sima, D. Matei, S. Condello, The outside-in journey of tissue transglutaminase in cancer, *Cells* 11 (2022) 1–24.
- [32] A. Shinde, J.S. Paez, S. Libring, K. Hopkins, L. Solorio, M.K. Wendt, Transglutaminase-2 facilitates extracellular vesicle-mediated establishment of the metastatic niche, *Oncogenesis* 9 (2020) 1–12.
- [33] B. Yakubov, L. Chen, A.M. Belkin, S. Zhang, B. Chelladurai, Z.Y. Zhang, D. Matei, Small molecule inhibitors target the tissue transglutaminase and fibronectin interaction, *PLoS One* 9 (2014) 1–10.
- [34] L.E. Sima, B. Yakubov, S. Zhang, S. Condello, A.A. Grigorescu, N.G. Nwani, L. Chen, G.E. Schiltz, C. Arvanitis, Z.Y. Zhang, D. Matei, Small molecules target the interaction between tissue transglutaminase and fibronectin, *Mol. Cancer Ther.* 18 (2019) 1057–1068.
- [35] May Khanna, Bhadrani Chelladurai, Aruna Gavini, Liwei Li, Minghai Shao, David Courtney, John J. Turchi, Targeting ovarian tumor cell adhesion mediated by tissue transglutaminase, *Mol. Cancer Ther.* 10 (2011) 626–636.
- [36] J.W. Keillor, K.Y.P. Apperley, A Akbar, Inhibitors of tissue transglutaminase, *Trends Pharmacol. Sci.* 36 (2015) 32–40.
- [37] D.M. Pinkas, P. Strop, A.T. Brunger, C. Khosla, Transglutaminase 2 undergoes a large conformational change upon activation, *PLoS Biol.* 5 (2007) 2788–2796.
- [38] S. Liu, R.A. Cerione, J. Clardy, Structural basis for the guanine nucleotide-binding activity of tissue transglutaminase and its regulation of transamidation activity, *Proc. Natl. Acad. Sci. U.S.A.* 99 (2002) 2743–2747.
- [39] R. Király, M.A. Demény, L. Fésüs, Protein transamidation by transglutaminase 2 in cells: a disputed Ca²⁺-dependent action of a multifunctional protein, *FEBS J.* 278 (2011) 4717–4739.
- [40] J. Stammaes, D.M. Pinkas, B. Fleckenstein, C. Khosla, L.M. Sollid, Redox regulation of transglutaminase 2 activity, *J. Biol. Chem.* 285 (2010) 25402–25409.
- [41] R. Iversena, S. Myslingb, K. Hnidaa, T.J.D. Jørgensenb, L.M. Sollida, Activity-regulating structural changes and autoantibody epitopes in transglutaminase 2 assessed by hydrogen/deuterium exchange, *Proc. Natl. Acad. Sci. U.S.A.* 111 (2014) 17146–17151.
- [42] P. Mariani, F. Carsughi, F. Spinozzi, S. Romanzetti, G. Meier, R. Casadio, C. M. Bergamini, Ligand-induced conformational changes in tissue transglutaminase: Monte Carlo analysis of small-angle scattering data, *Biophys. J.* 78 (2000) 3240–3251.
- [43] R. Staffler, R. Pasternack, M. Hils, W. Kaiser, F.M. Möller, Nucleotide binding kinetics and conformational change analysis of tissue transglutaminase with switchSENSE, *Anal. Biochem.* 605 (2020) 1–7.
- [44] I. Cardoso, E.C. Østerlund, J. Stammaes, R. Iversen, J.T. Andersen, T.J. D. Jørgensen, L.M. Sollid, Dissecting the interaction between transglutaminase 2 and fibronectin, *Amino Acids* 49 (2017) 489–500.
- [45] M.F. Soluri, F. Boccafoschi, D. Cotella, L. Moro, G. Forestieri, I. Autiero, L. Cavallo, R. Oliva, M. Griffin, Z. Wang, C. Santoro, D. Sblattero, Mapping the minimum domain of the fibronectin binding site on transglutaminase 2 (TG2) and its importance in mediating signaling, adhesion, and migration in TG2-expressing cells, *FASEB J.* 33 (2019) 2327–2342.
- [46] P.M. Turner, L. Lorand, Complexation of fibronectin with tissue transglutaminase*, *Annu. Rev. Physiol.* 28 (1989) 688–691.
- [47] J.M. Jeong, S.N.P. Murthy, J.T. Radek, L. Lorand, The fibronectin-binding domain of transglutaminase, *J. Biol. Chem.* 270 (1995) 5654–5658.
- [48] J. Hang, E.A. Zemskov, L. Lorand, A.M. Belkin, Identification of a novel recognition sequence for fibronectin within the NH2-terminal β -sandwich domain of tissue transglutaminase, *J. Biol. Chem.* 280 (2005) 23675–23683.
- [49] J.T. Radek, J.-M. Jeong, S.N. Prasanna Murthy, K.C. Ingham, L. Lorand, Affinity of human erythrocyte transglutaminase for a 42-kDa gelatin-binding fragment of human plasma fibronectin, *Proc. Natl. Acad. Sci. U.S.A.* 90 (1993) 3152–3156.
- [50] N.I. Abu-Lail, T. Ohashi, R.L. Clark, H.P. Erickson, S. Zauscher, Understanding the elasticity of fibronectin fibrils: unfolding strengths of FN-III and GFP domains measured by single molecule force spectroscopy, *Matrix Biol.* 25 (2006) 175–184.
- [51] M.L. Smith, D. Gourdon, W.C. Little, K.E. Kubow, R.A. Eguiluz, S. Luna-morris, V. Vogel, Force-induced unfolding of fibronectin in the extracellular matrix of living cells, *PLoS Biol.* 5 (2007) 2243–2254.
- [52] L.M. Maurer, W. Ma, D.F. Mosher, Dynamic structure of plasma fibronectin, *Crit. Rev. Biochem. Mol. Biol.* 51 (2016) 213–227.
- [53] J.E. Schwarzbauer, D.W. DeSimone, Fibronectins, their fibrillogenesis, and in vivo functions, *Cold Spring Harb. Perspect. Biol.* 3 (2011) 1–19.
- [54] S.M. Früh, I. Schoen, J. Ries, V. Vogel, Molecular architecture of native fibronectin fibrils, *Nat. Commun.* 6 (2015) 1–10.
- [55] V. Vogel, Unraveling the mechanobiology of extracellular matrix, *Annu. Rev. Physiol.* 80 (2018) 353–387.
- [56] K.C. Ingham, S.A. Brew, S. Huff, S.V. Litvinovich, Cryptic self-association sites in type III modules of fibronectin, *J. Biol. Chem.* 272 (1997) 1718–1724.
- [57] C. Zhong, M. Chrzanowska-Wodnicka, J. Brown, A. Shaub, A.M. Belkin, K. Burridge, Rho-mediated contractility exposes a cryptic site in fibronectin and induces fibronectin matrix assembly, *J. Cell Biol.* 141 (1998) 539–551.
- [58] D.C. Hocking, J. Sottile, P.J. McKeown-Longo, Fibronectin's 111-1 module contains a conformation-dependent binding site for the amino-terminal region of fibronectin, *J. Biol. Chem.* 269 (1994) 19183–19191.
- [59] W.C. Little, M.L. Smith, U. Ebnetner, V. Vogel, Assay to mechanically tune and optically probe fibrillar fibronectin conformations from fully relaxed to breakage, *Matrix Biol.* 27 (2008) 451–461.
- [60] M. Chabria, S. Hertig, M.L. Smith, V. Vogel, Stretching fibronectin fibres disrupts binding of bacterial adhesins by physically destroying an epitope, *Nat. Commun.* 1 (2010) 1–9.
- [61] K.E. Kubow, R. Vukmirovic, L. Zhe, E. Klotzsch, M.L. Smith, D. Gourdon, S. Luna, V. Vogel, Mechanical forces regulate the interactions of fibronectin and collagen I in extracellular matrix, *Nat. Commun.* 6 (2015) 1–11.
- [62] Y. Wang, J. Yan, B.T. Goult, Force-dependent binding constants, *Biochemistry* 58 (2019) 4696–4709.
- [63] D. Ortiz Franyuti, M. Mitsi, V. Vogel, Mechanical stretching of fibronectin fibers upregulates binding of interleukin-7, *Nano Lett.* 18 (2018) 15–25.
- [64] E.W. Deutsch, N. Bandeira, Y. Perez-Riverol, V. Sharma, J.J. Carver, L. Mendoza, D.J. Kundu, S. Wang, C. Bandla, S. Kamatchinathan, S. Hewapathirana, B. S. Pullman, J. Wertz, Z. Sun, S. Kawano, S. Okuda, Y. Watanabe, B. Maclean, M. J. Maccoss, Y. Zhu, Y. Ishihama, J.A. Vizcaino, The ProteomeXchange consortium at 10 years: 2023 update, *Nucleic Acids Res.* 51 (2023) D1539–D1548.
- [65] B. Vallat, B. Webb, M. Fayazi, S. Voinea, H. Tangmunarunkit, S.J. Ganesan, C. L. Lawson, J.D. Westbrook, C. Kesselman, A. Sali, H.M. Berman, New system for archiving integrative structures, *Acta Cryst.* 77, (Pt 12) (2021) 1486–1496.
- [66] S. Hertig, M. Chabria, V. Vogel, Engineering mechanosensitive multivalent receptor-ligand interactions: why the nanolinker regions of bacterial adhesins matter, *Nano Lett.* 12 (2012) 5162–5168.
- [67] Enrico Klotzsch, Michael L. Smith, Kristopher E. Kubow, Simon Muntwyler, William C. Little, Felix Beyeler, Delphine Gourdon, Bradley J. Nelson, Fibronectin forms the most extensible biological fibers displaying switchable force-exposed cryptic binding sites, *Proc. Natl. Acad. Sci.* 106 (2009) 18267–18272.
- [68] G. Baneyx, L. Baugh, V. Vogel, Fibronectin extension and unfolding within cell matrix fibrils controlled by cytoskeletal tension, *PNAS* 99 (2002) 5139–5143.
- [69] G. Baneyx, L. Baugh, V. Vogel, Coexisting conformations of fibronectin in cell culture imaged using fluorescence resonance energy transfer, *PNAS* 98 (2001) 14464–14468.
- [70] W.C. Little, R. Schwartlander, M.L. Smith, D. Gourdon, V. Vogel, Stretched extracellular matrix proteins turn fouling and are functionally rescued by the chaperones albumin and casein, *Nano Lett.* 9 (2009) 4158–4167.
- [71] X. Jin, J. Stammaes, C. Klöck, T.R. DiRaimondo, L.M. Sollid, C. Khosla, Activation of extracellular transglutaminase 2 by thioredoxin, *J. Biol. Chem.* 286 (2011) 37866–37873.
- [72] O. Peleg, T. Savin, G.V. Kolmakov, I.G. Salib, A.C. Balazs, M. Kröger, V. Vogel, Fibers with integrated mechanochemical switches: minimalistic design principles derived from fibronectin, *Biophys. J.* 103 (2012) 1909–1918.
- [73] J. Stammaes, R. Iversen, M. Fleur Du Pré, X. Chen, L.M. Sollid, Enhanced B-cell receptor recognition of the autoantigen transglutaminase 2 by efficient catalytic self-multimerization, *PLoS One* 10 (2015) 1–19.
- [74] G.E. Begg, L. Carrington, P.H. Stokes, J.M. Matthews, M.A. Wouters, A. Husain, L. Lorand, S.E. Iismaa, R.M. Graham, Mechanism of allosteric regulation of transglutaminase 2 by GTP, *Proc. Natl. Acad. Sci. U.S.A.* 103 (2006) 19683–19688.
- [75] L. Piersimoni, P.L. Kastiris, C. Arlt, A. Sinz, Cross-linking mass spectrometry for investigating protein conformations and protein-protein interactions—a method for all seasons, *Chem. Rev.* 122 (2022) 7500–7531.
- [76] M. Grimm, T. Zimniak, A. Kahraman, F. Herzog, XViS: a web server for the schematic visualization and interpretation of crosslink-derived spatial restraints, *Nucleic Acids Res.* 43 (2015) W362–W369.
- [77] A. Graziadei, J. Rappsilber, Leveraging crosslinking mass spectrometry in structural and cell biology, *Structure* 30 (2022) 37–54.
- [78] Z. Orbán-Németh, R. Beveridge, D.M. Hollenstein, E. Rampler, T. Stranzl, O. Hudecz, J. Doblmann, P. Schögelhofer, K. Mechtler, Structural prediction of protein models using distance restraints derived from cross-linking mass spectrometry data, *Nat. Protoc.* 13 (2018) 478–494.
- [79] E. Rampler, T. Stranzl, Z. Orbán-Németh, D.M. Hollenstein, O. Hudecz, P. Schloegelhofer, K. Mechtler, Comprehensive cross-linking mass spectrometry reveals parallel orientation and flexible conformations of plant HOP2-MND1, *J. Proteome Res.* 14 (2015) 5048–5062.
- [80] J. Yang, Y. Zhang, Protein structure and function prediction using I-TASSER, *Curr. Protoc. Bioinforma.* 52 (2015), 5.8.1–5.8.15.
- [81] A. Kahraman, L. Malmström, R.Xwalk Aebersold, Computing and visualizing distances in cross-linking experiments, *Bioinformatics* 27 (2011) 2163–2164.
- [82] A. Leitner, L.A. Joachimiak, P. Unverdorben, T. Walzthoenl, J. Frydman, F. Förster, R. Aebersold, Chemical cross-linking/mass spectrometry targeting acidic residues in proteins and protein complexes, *Proc. Natl. Acad. Sci. U.S.A.* 111 (2014) 9455–9460.
- [83] D.E. Kim, D. Chivian, D. Baker, Protein structure prediction and analysis using the Robetta server, *Nucleic Acids Res.* 32 (2004) W526–W531.
- [84] M. MirDita, K. Schütze, Y. Moriwaki, L. Heo, S. Ovchinnikov, M. Steinegger, ColabFold: making protein folding accessible to all, *Nat. Methods* 19 (2022) 679–682.
- [85] P. Benkert, M. Biasini, T. Schwede, Toward the estimation of the absolute quality of individual protein structure models, *Bioinformatics* 27 (2011) 343–350.
- [86] G.C.P. Van Zundert, J.P.G.L.M. Rodrigues, M. Trellet, C. Schmitz, P.L. Kastiris, E. Karaca, A.S.J. Melquiond, M. Van Dijk, S.J. De Vries, A.M.J.J. Bonvin, The HADDOCK2.2 web server: user-friendly integrative modeling of biomolecular complexes, *J. Mol. Biol.* 428 (2016) 720–725.

- [87] G.C.P. Van Zundert, A.M.J.J. Bonvin, DisVis: Quantifying and visualizing accessible interaction space of distance-restrained biomolecular complexes, *Bioinformatics* 31 (2015) 3222–3224.
- [88] S. Hubbard, NACCESS, Computer Program, J.T., Department of Biochemistry and Molecular Biology, University College, London, 1993. at
- [89] M. Le, C. Erat, D.A. Slatter, E.D. Lowe, C.J. Millard, R.W. Farndale, I.D. Campbell, I. Vakonakis, Identification and structural analysis of type I collagen sites in complex with fibronectin fragments, *PNAS* 17 (2009) 4195–4200.
- [90] H. Lindmark, B. Guss, SFS, a novel fibronectin-binding protein from *Streptococcus equi*, inhibits the binding between fibronectin and collagen, *Infect. Immun.* 67 (1999) 2383–2388.
- [91] W. Ma, H. Ma, F.J. Fogerty, D.F. Mosher, Bivalent ligation of the collagen-binding modules of fibronectin by SFS, a non-anchored bacterial protein of *streptococcus equi*, *J. Biol. Chem.* 290 (2015) 4866–4876.
- [92] LeMosyos, E.K., Erickson, H.P., Beyer, W.F., Radek, J.T., Jeong, J.-M., Murthy, S.N. P. & Lorand, L. Visualization of purified fibronectin-transglutaminase complexes*. 267, 7880–7885 (1992).
- [93] A. Janiak, E.A. Zemskov, A.M. Belkin, Cell surface transglutaminase promotes RhoA activation via integrin clustering and suppression of the Src-p190RhoGAP signaling pathway, *Mol. Biol. Cell* 17 (2006) 1606–1619.
- [94] C.D. Müller, G. Ruiz-Gómez, S. Cazzonelli, S. Möller, R. Wodtke, R. Löser, J. Freyse, J.-N. Dürig, J. Rademann, U. Hempel, M.T. Pisabarro, S. Vogel, Sulfated glycosaminoglycans inhibit transglutaminase 2 by stabilizing its closed conformation, *Sci. Rep.* 12 (2022) 1–16.
- [95] H. Lortat-Jacob, I. Burhan, A. Scarpellini, A. Thomas, A. Imberty, R.R. Vivès, T. Johnson, A. Gutierrez, E.A.M. Verderio, Transglutaminase-2 interaction with heparin: identification of a heparin binding site that regulates cell adhesion to fibronectin-transglutaminase-2 matrix, *J. Biol. Chem.* 287 (2012) 18005–18017.
- [96] M. Satpathy, L. Cao, R. Pincheira, R. Emerson, R. Bigsby, H. Nakshatri, D. Matei, Enhanced peritoneal ovarian tumor dissemination by tissue transglutaminase, *Cancer Res.* 67 (2007) 7194–7202.
- [97] M.E. Van Strien, B. Drukarch, J.G. Bol, P. Van Der Valk, J. Van Horsen, W. H. Gerritsen, J.J. Breve, A.M. Van Dam, Appearance of tissue transglutaminase in astrocytes in multiple sclerosis lesions: a role in cell adhesion and migration? *Brain Pathol.* 21 (2011) 44–54.
- [98] M.E. van Strien, J.J.P. Brevé, S. Fratantoni, M.W.J. Schreurs, J.G.J.M. Bol, C.A. M. Jongenelen, B. Drukarch, A.M. van Dam, Astrocyte-derived tissue transglutaminase interacts with fibronectin: a role in astrocyte adhesion and migration? *PLoS One* 6 (2011) 1–12.
- [99] N. Espitia Pinzón, J.J.P. Brevé, J.G.J.M. Bol, B. Drukarch, W. Baron, A.M. van Dam, Tissue transglutaminase in astrocytes is enhanced by inflammatory mediators and is involved in the formation of fibronectin fibril-like structures, *J. Neuroinflammation* 14 (2017) 1–13.
- [100] N. Espitia Pinzón, B. Sanz-Morello, J.J.P. Brevé, J.G.J.M. Bol, B. Drukarch, J. Bauer, W. Baron, A.M. Van Dam, Astrocyte-derived tissue transglutaminase affects fibronectin deposition, but not aggregation, during cuprizone-induced demyelination, *Sci. Rep.* 7 (2017) 1–13.
- [101] L. Yuan, M. Siegel, K. Choi, C. Khosla, C.R. Miller, E.N. Jackson, D. Piwnicka-Worms, K.M. Rich, Transglutaminase 2 inhibitor, KCC009, disrupts fibronectin assembly in the extracellular matrix and sensitizes orthotopic glioblastomas to chemotherapy, *Oncogene* 26 (2007) 2563–2573.
- [102] I. Cardoso, J. Stamnaes, J.T. Andersen, G. Melino, R. Iversen, L.M. Sollid, Transglutaminase 2 interactions with extracellular matrix proteins as probed with celiac disease autoantibodies, *FEBS J.* 282 (2015) 2063–2075.
- [103] G. Singh, J. Zhang, Y. Ma, R.A. Cerione, M.A. Antonyak, The different conformational states of tissue transglutaminase have opposing effects on cell viability, *J. Biol. Chem.* 291 (2016) 9119–9132.
- [104] N. Kim, W.K. Lee, S.H. Lee, K.S. Jin, K.H. Kim, Y. Lee, M. Song, S.Y. Kim, Inter-molecular crosslinking activity is engendered by the dimeric form of transglutaminase 2, *Amino Acids* 49 (2017) 461–471.
- [105] C.M. Fonta, S. Arnoldini, D. Jaramillo, A. Moscaroli, A. Oxenius, M. Behe, V. Vogel, Fibronectin fibers are highly tensed in healthy organs in contrast to tumors and virus-infected lymph nodes, *Matrix Biol. Plus* 8 (2020) 1–15.
- [106] K. Hnida, J. Stamnaes, M.F. Du Pré, S. Mysling, T.J.D. Jørgensen, L.M. Sollid, R. Iversen, Epitope-dependent functional effects of celiac disease autoantibodies on transglutaminase 2, *J. Biol. Chem.* 291 (2016) 25542–25552.
- [107] M.C. Benn, S.A. Pot, J. Moeller, T. Yamashita, C.M. Fonta, G. Orend, P. Kollmannsberger, V. Vogel, How the mechanobiology orchestrates the iterative and reciprocal ECM-cell cross-talk that drives microtissue growth, *Sci. Adv.* 9 (2023) 1–19.
- [108] C.M. Fonta, T. Loustau, C. Li, S.P. Surendran, U. Hansen, D. Murdamoothoo, M. C. Benn, I. Velazquez-Quesada, R. Carapito, G. Orend, V. Vogel, Infiltrating CD8+ T cells and M2 macrophages are retained in tumor matrix tracks enriched in low tension fibronectin fibers, *Matrix Biol.* 116 (2023) 1–27.
- [109] S.A. Pot, Z. Lin, J. Shiu, M.C. Benn, V. Vogel, Growth factors and mechano-regulated reciprocal crosstalk with extracellular matrix tune the keratocyte–fibroblast/myofibroblast transition, *Sci. Rep.* 13 (2023) 1–19, 2023 131.
- [110] F. Klingberg, M.L. Chow, A. Koehler, S. Boo, L. Buscemi, T.M. Quinn, M. Costell, B.A. Alman, E. Genot, B. Hinz, Prestress in the extracellular matrix sensitizes latent TGF- β 1 for activation, *J. Cell Biol.* 207 (2014) 283–297.
- [111] Klingberg, F., Chau, G., Walraven, M., Boo, S., Koehler, A., Chow, M.L., Olsen, A. L., Im, M., Lodyga, M., Wells, R.G., White, E.S. & Hinz, B. The fibronectin ED-a domain enhances recruitment of latent TGF- β -binding protein-1 to the fibroblast matrix. (2018) doi:10.1242/jcs.201293.
- [112] D.J. Tschumperlin, D. Lagares, Mechano-therapeutics: targeting mechanical signaling in fibrosis and tumor stroma, *Pharmacol. Ther.* 212 (2020) 107575.
- [113] J. Sottile, F. Shi, I. Rublyevska, H.Y. Chiang, J. Lust, J. Chandler, Fibronectin-dependent collagen I deposition modulates the cell response to fibronectin, *Am. J. Physiol. - Cell Physiol.* 293 (2007) 1934–1946.
- [114] J. Van Rheenen, M. Langeslag, K. Jalink, Correcting confocal acquisition to optimize imaging of fluorescence resonance energy transfer by sensitized emission, *Biophys. J.* 86 (2004) 2517–2529.
- [115] A. Leitner, T. Walzthoeni, R. Aebersold, Lysine-specific chemical cross-linking of protein complexes and identification of cross-linking sites using LC-MS/MS and the xQuest/xProphet software pipeline, *Nat. Protoc.* 9 (2014) 120–137.
- [116] A. Mohammadi, A. Tschanz, A. Leitner, Expanding the cross-link coverage of a carboxyl-group specific chemical cross-linking strategy for structural proteomics applications, *Anal. Chem.* 93 (2021) 1944–1950.
- [117] T. Walzthoeni, M. Claassen, A. Leitner, F. Herzog, S. Bohn, F. Förster, M. Beck, R. Aebersold, False discovery rate estimation for cross-linked peptides identified by mass spectrometry, *Nat. Methods* 9 (2012) 901–903.
- [118] E.F. Pettersen, T.D. Goddard, C.C. Huang, E.C. Meng, G.S. Couch, T.I. Croll, J. H. Morris, T.E. Ferrin, UCSF ChimeraX: structure visualization for researchers, educators, and developers, *Protein Sci.* 30 (2021) 70–82.
- [119] Y. Perez-Riverol, J. Bai, C. Bandla, D. García-Seisdedos, S. Hewapathirana, S. Kamatchinathan, D.J. Kundu, A. Prakash, A. Frericks-Zipper, M. Eisenacher, M. Walzer, S. Wang, A. Brazma, J.A. Vizcaíno, The PRIDE database resources in 2022: a hub for mass spectrometry-based proteomics evidences, *Nucleic. Acids. Res.* 50 (2022) D543–D552.